Gondwana Research 110 (2022) 73–89

Contents lists available at ScienceDirect

Gondwana Research

journal homepage: www.elsevier.com/locate/gr

Ferruginous biofilm preservation of *Ediacaran* fossils

G.J. Retallack

Department of Geological Sciences, University of Oregon, Eugene, OR, USA

ARTICLE INFO

Article history:
Received 21 February 2022
Revised 8 April 2022
Accepted 15 June 2022
Available online 18 June 2022
Handling Editor: J.G. Meert

Keywords:
Taphonomy
Biofilm
Hematite
Pyrite
Ediacaran

ABSTRACT

Ferruginous biofilms are a form of preservation of fossil leaves making detailed imprints of venation even in coarse sandstone. In modern examples, the biofilm is robust enough to persist after separation, or rotting of the leaf. The biofilms are created by filamentous, iron-oxidizing bacteria such as *Leptothrix* and *Sphaerotilus*, and have distinctive felted microscopic textures. Ediacaran vendobionts with fine detail preserved in coarse sandstone show these diagnostic felted textures under the scanning electron microscope. These biofilms were thus pre-depositional ferruginous death masks, and lack distinctive framboidal textures or pyritohedral textures of pyrite. Pyritic external-only "death masks" are undocumented from any geological age or locality. Ediacaran fossils are also preserved by silica permineralization, silica-cemented molds and casts, and pyrite permineralization and replacement after burial. This examination of unskeletonized Ediacaran fossils from Australia, Russia, Namibia, California, and Newfoundland in thin section and scanning electon microscope shows no evidence for a uniquely Ediacaran style of fossil preservation.

1. Introduction

The iconic unskeletonized, quilted, Ediacaran fossils known as vendobionts present a preservational conundrum, because they have been interpreted as animals preserved in organic-poor sandstones with high relief (Seilacher, 1989). Low-relief, soft-bodied fossils are known in black shales, siderite and limestone of Ediacaran (Xiao et al., (2002; Grazhdankin et al., 2008; Bykova et al., 2017), and Phanerozoic age (Schopf, 1975; Hou et al., 2008; Retallack, 2011). In Phanerozoic sandstones the only unskeletonized fossils preserved in this way are plants, arthropods, and dried dinosaur skin with tough biopolymers (Hall et al., 1988; McNamara and Trewin, 1993; Gastaldo, 1992; Retallack, 1994; Anderson et al., 1998; Paik et al., 2010; Retallack and Dilcher, 2012; Barth et al., 2013; MacGabhann et al., 2019), and other vendobiont-like fossils of uncertain affinities (Glaessner, 1979; Hagadorn et al., 2000, 2002; Jensen et al., 1998; MacGabhann et al., 2019; Retallack, 2018).

One solution to high fidelity preservation of leaves in sandstone is pre-depositional ferruginous death masks, observed from iron-oxidizing bacterial biofilms (Fig. 1A-C. E) of filamentous bacteria (Fig. 2C-D) on modern leaves (Fig. 1A-C,E: Dunn et al., 1997; Spicer, 1977). Comparable ferruginous death masks also are known from fossils (Fig. 3F-G, Fig. 4A-B: Retallack and Dilcher, 2012; Locatelli et al., 2017), and have a characteristic felted microtexture (Fig. 5A-H). These clayey oxidized biofilms of lakes and soils are distinct from coarsely crystalline chlorite films found on marine fossil compressions (Gámez Vintaned et al., 2011; Wan et al., 2020; Becker-Kerber et al., 2022). They are further evidence for non-marine habitats of some Ediacaran fossils (Retallack, 2013b, 2016a).

An alternative solution to high relief preservation of soft-bodied fossils is the hypothesis of pyrite death masks, compaction-resistant mineral rinds, preserving both the outline and relief of the fossil exterior, but not its interior (Gehling, 1999; Liu, 2016). Pyritization is formed by sulfate-reducing bacteria (Fig. 2A-B) active while organic matter was still present as fuel to permineralize and fill fossils (Fig. 3A-D). Pyritization has a distinct micromophology of spherical framboids or angular pyritohedra (Fig. 5I-P). A real death mask is a thick (2–3 cm) layer of plaster applied to the face of the deceased to make a three-dimensional replica: by definition, it does not penetrate the face or its cavities, and oil is used to prevent hair entanglement (Kaufman and McNeil, 1989). The idea of pyritic death masks is fine in theory, but no one has ever found an exterior-only, death mask of interlocking, rigid, pyrite on a fossil (Liu et al., 2019; Tarhan et al., 2016, 2017). Both Ediacaran and Phanerozoic fossils are pyritized internally to varying degrees, but have external pyrite only when completely filled with pyrite (Liu, 2016; Retallack, 2016b). Lack of pyrite in almost all Australian Ediacaran fossils has been attributed to oxidation of pyrite in outcrop (Mapstone and McIlroy, 2006; Tarhan et al., 2015). If that were true there should be remaining framboidal,

E-mail address: gregr@uoregon.edu

https://doi.org/10.1016/j.gr.2022.06.007
1342-937X/

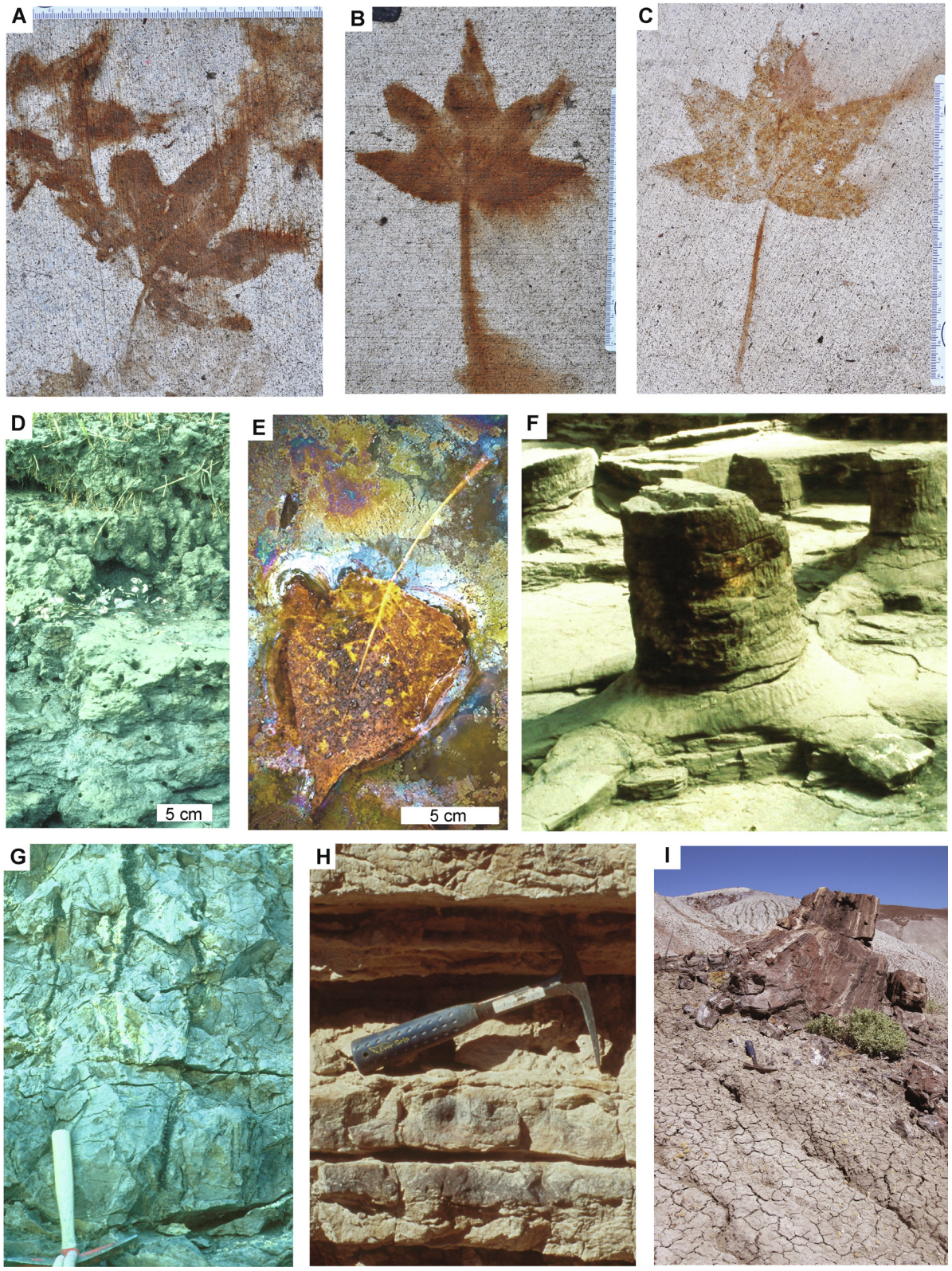

Fig. 1. Modern (A-F) and deep time (G-I) terrestrial environments of pyritization (D,G), ferruginous biofilms (A-C,E, H) and silicification (F,I); A-C, ferruginous biofilms of leaves of sweet gum (*Liquidambar styraciflua*) on concrete pavement near Erb Memorial Union, University of Oregon November 30, 2020; D, gleyed soil with pyritic horizon below clams (*Brachidontes modiolus*) and humic surface with salt grass (*Spartina alterniflora*) on Bass Creek, Kiawah Island, South Carolina; E, leaf (*Populus tremuloides*) with ferruginous encrustation, Holland Ponds, Shelby, Michigan; F, stump (*Stigmaria ficoides*) with uncompressed roots in a clayey paleosol (Fluvent) of the Limestone Coal Formation of Carboniferous (Namurian) age in Victoria Park, Glasgow; G, pyritized root traces (shining and golden) in Bg horizon of gray Makizi pedotype of Cretaceous (Cenomanian) Dakota Formation in Cloud Ceramic Company pit south of Concordia, Kansas; H, leaf-bearing surface horizon of weakly developed sandy Sagi paleosol (in sun immediately below hammer) in levee facies, Cretaceous (Cenomanian), Dakota Formation in Kansas Brick and Tile Company pit south of Hoisington, Kansas; I, stump (*Pullisylvanoxylon arizonicum*) in growth position within A horizon of purple Azid pedotype, Triassic (Norian), Blue Mesa Member, Chinle Formation, near Tepee Buttes, Petrified Forest National Park, Arizona. Image B is from Mark Graf with permission. (For interpretation of the references to color in this figure legend, the reader is referred to the web version of this article.)

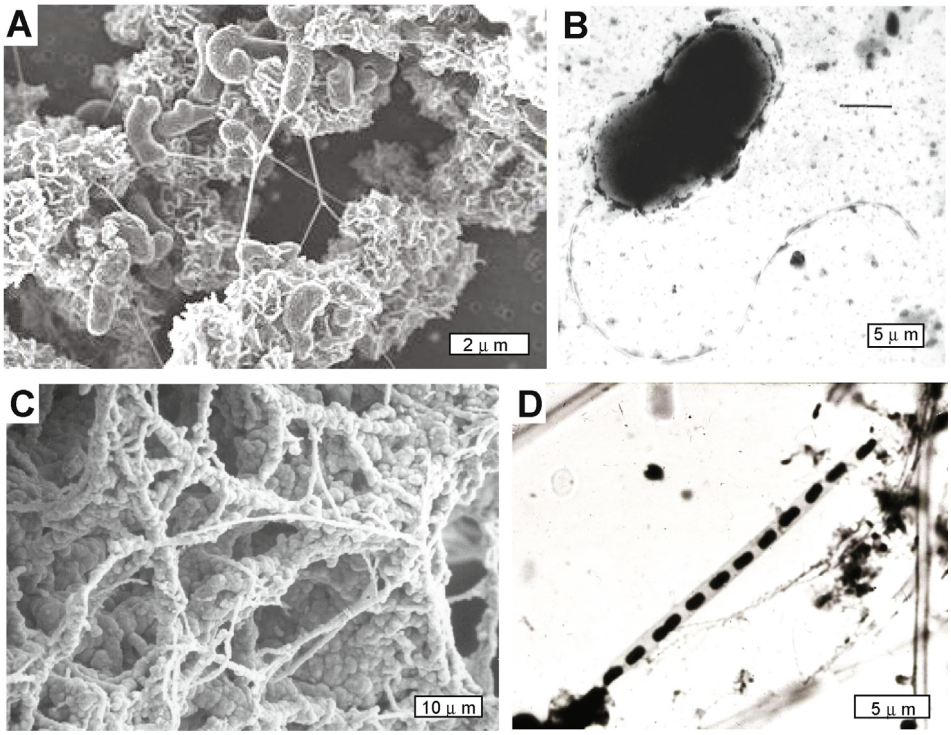

Fig. 2. Vibrio-shaped, sulfate-reducing bacteria are replacive, creating pits filled with pyrite, whereas filamentous iron-oxidizing bacteria form surface biofilms: sulfate-reducing vibrio *Desulfovibrio vulgaris* (A-B), and iron-oxidizing filaments *Leptothrix ochracea* (C-D) in scanning electon microscopy (A,C) and light microscopy (B,D). Sources are (A) bacilli on corroded metal surface from Weiwen Zhang and Fred Bockman, with permission; (B) by Graham Bradley, with permission; (C) by Fred Luiszer, with permission; and D) by Brudersohn with permission.

pyritohetral, or cubic molds. At issue is whether surficial hematite encrustations of Ediacaran fossils were originally ferric oxyhydrates or pyrite, and this question is addressed here with comprehensive petrographic and scanning electron microscopic studies.

If pyritic exterior-only death masks existed, as opposed to common pyritic replacement, permineralization, and nodularization (Gan et al., 2021; Liu, 2016; MacGabhann et al., 2019), they would have been a uniquely Ediacaran style of preservation, explained by Gehling (1999) as due to sedimentary oxidation through the post-Ediacaran evolution of marine bioturbation. Similarly, Tarhan et al. (2016) and Slagter et al. (2020) propose that animals were not silica-cemented after the Ediacaran because marine silica concentrations were biologically depleted during the Phanerozoic. These claims of uniquely Ediacaran styles of fossil preservation are also addressed here with examination of both Ediacaran and Phanerozoic fossil preservation, to evaluate the null hypothesis that Ediacaran fossils were preserved in the same ways as Phanerozoic fossils (MacGabhann et al., 2019; Retallack, 1994, 2007).

2. Materials and methods

This study examined large collections of fossils (Table 1) as hand specimens (Fig. 3), in thin section (Fig. 4), and under the scanning electron microscope (Figs. 5-6). Ediacaran fossils were examined from the Ediacara Member of the Rawnsley Quartzite in the Flinders Ranges, South Australia (Fig. 3E; Retallack, 1994, 2007, 2013b), the Arumbera and Grant Bluff Formations of Northern Territory (Glaessner and Walter, 1975; Mapstone and McIlroy, 2006; Retallack and Broz, 2020a, 2020b, Wade, 1969), the Drook, Mistaken Point, and Fermeuse Formations of Newfoundland (Fig. 3A; Gehling et al., 2000; Retallack, 2014, 2016b, 2016c), the Cambridge Argillite of Massachusetts (Bailey 1987; Retallack, 2022), the Dabis Formation of Namibia (Fig. 3H; Pflug, 1973, 1994; Vickers-Rich et al., 2013, 2016), the Bradgate Formation of England (Carney et al., 2008), and the Dengying Formation of China (Cao et al., 2010). Also included was examination of 96 specimens of *Dickinsonia* reported by Retallack (2007: collection of South Australian Museum, Adelaide), and 6 specimens of *Arumberia* reported by Glaessner and Walter (1975) and Retallack and Broz (2020a: collection of Geoscience Australia, Canberra). The FEI Qanta ESEM-VPSEM scanning electron microscope at the University of Oregon CAMCOR facility was used to examine Ediacaran sandstone fossils under both back-scatter, which presents atomic number as a tone (Fig. 5), and under secondary electron beam, giving relief form only (Figs. 5-6). Pyrite appears bright white under back-scatter, but hematite, clay and other silicate minerals are gray (Ohfuji et al., 2005).

3. Ferruginous biofilms

3.1. Ediacaran ferruginization

Ediacaran fossils with hematite encrustation are common among classic fossils of South Australia (Gehling, 1999; Retallack, 2007), central Australia (Mapstone and McIlroy, 2006; Retallack and Broz, 2020a, 2020b), and India (Retallack et al. 2021). *Dickinsonia* for example shows unusually detailed texture for sandstone casts, compared with areas of sandstone matrix away from the fossil (Fig. 3E). The detailed upper surface of the fossil is preserved as a concave hyporelief in the overlying slab in most fossils, and has a thick, upper rind of hematite (Fig. 4A-B), which appears smooth to striated and tufted under the scanning electron microscope (Fig. 5-A-B, 6A-B). Interior seams and less detailed convex impressions of the lower surface of the fossil on the substrate are also oxidized with hematite, but are less strongly ferruginized than the upper

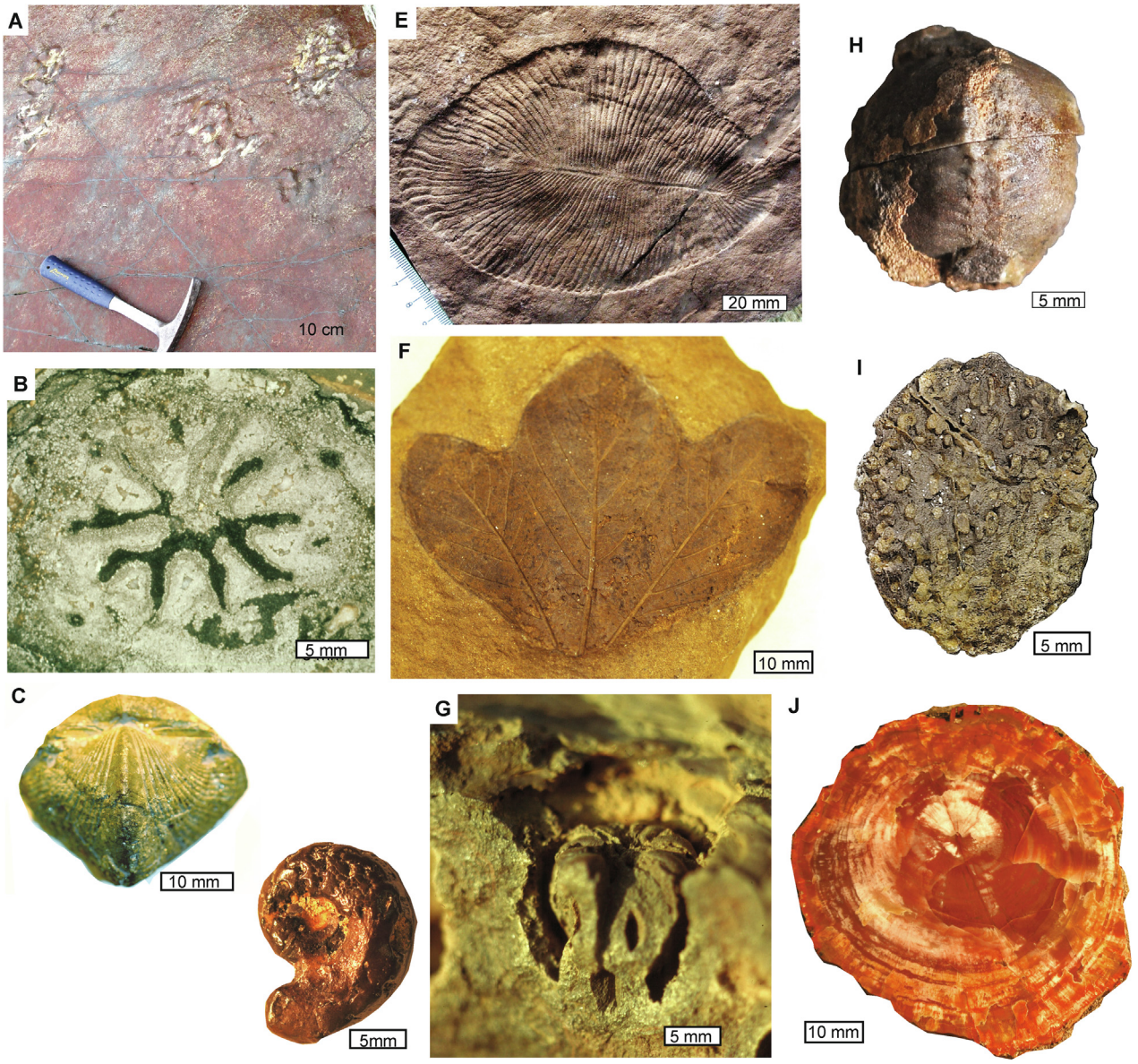

Fig. 3. Fossils preserved by pyritization (A – D), ferruginous biofilms (E – G), and silicification (H – J) in the Ediacaran (A,E,H) and Phanerozoic (B – D, F - G, I - J): A, *Ivesheadia lobata*, Ediacaran, Drook Formation, Drook, Newfoundland; B, cross section of *Langoxylon asterochlaenoideum*, Devonian (Givetian), Bois de Bordeaux Formation, Ronquiéres, Belgium; C, *Paraspirifer brownockeri*, Devonian (Givetian), Silica Shale, Sylvania, Ohio; D, *Myloceras joffrei*, Cretaceous (late Albian), Wangarlu Mudstone, Harneys Beach, Northern Territory, Australia; E, *Dickinsonia costata*, Ediacaran, Ediacara Member, Rawnsley Quartzite, Ediacara Hills, South Australia; F, *Araliopsoides cretacea*, Cretaceous (Cenomanian), Dakota Formation, Ellsworth, Kansas; G, *Dakotanthus cordiformis*, Cretaceous (Cenomanian), Dakota Formation, Ellsworth, Kansas; H, *Ernettia plateauensis*, Ediacaran, Kuibis Formation, Aus, Namibia; I, *Palaeophytocrene foveolata*, Eocene (Lutetian), Clarno Formation, Clarno Nut Beds, Clarno, Oregon; J, *Pullisylvanoxylon arizonicum*, Triassic (Norian), St Johns, Arizona. Panel A is a field photograph, and specimen numbers in Condon Collection of Museum of Natural and Cultural History, University of Oregon are F114846 (C), F117299 (D), F113777 (K), F109381 (I), F111197 (J); of Institute Royal des Sciences Naturelles, Brussels 107,303 courtesy of Stephen Scheckler (B); of the South Australian Museum, Adelaide is F17462 (E); of Thomas Burke Memorial Museum, University of Washington is PB17535 (F); of University of Florida Natural History Museum is 3428 (G).

surface (Fig. 4A-B; Gehling, 1999; Retallack, 2007; Evans et al., 2019). These interior structures and lower surface are evidence against rheotrophic deformation of sediment into the dome of the upper rind, as proposed by Wade (1968) and Bobrovskiy et al. (2019). Sediment infiltrated a system of chambers opened by partial decay and does not show rheid folding. Fossils such as *Dickinsonia*, *Tribrachidium* and *Parvancorina*, show resistance to burial compaction, unlike collapse found in discoid Ediacaran fossils on the same slabs (Gehling, 1999; Reid et al., 2017; Retallack, 1994, 2016b). Yet the resistant fossils, as well as the collapsed discoids, and the elephant-skin textured surface bearing the fossils are often coated in felted hematite (Retallack, 2013a, 2016b). These are indications that the fossils, as well as textured microbial surfaces around them, were enriched in iron before burial.

One explanation for these hematite rinds is that they were oxidized from pyritic death masks in current outcrop (Gehling, 1999; Mapstone and McIlroy, 2006; Tarhan et al. 2015), and that possibility was tested here by searching for relict molds of pyritohedra or framboids in Ediacaran ferruginized fossils using the scanning electron microscope. Scanning of 106 red bed specimens from the Ediacara Member of South Australia and the Arumbera Formation of central Australia failed to find any pits or molds of pyritohedra or framboids (Fig. 5A-B, 6A-D). None of the ferruginised Ediacaran fossils showed pyritohedra, framboids, or pseudomorphs of them,

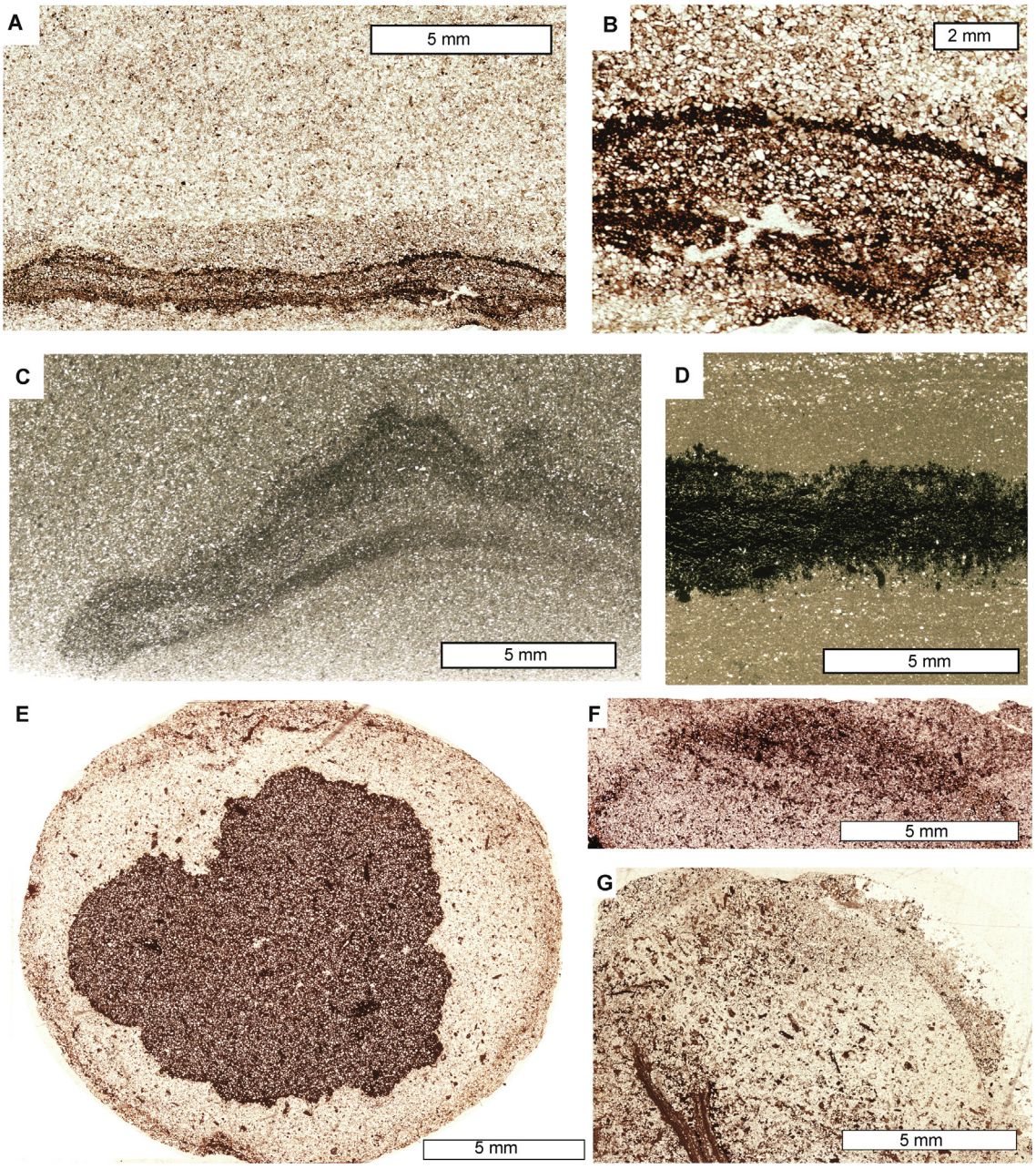

Fig. 4. Three distinct styles of Edicaran fossil preservation in petrographic thin sections: A-B, ferruginous biofilms from the Ediacara Member of the Rawnsley Quartzite in Brachina Gorge, South Australia; C-D, partial pyrite replacement of organic matter from the Mistaken Point Formation at St Shotts, and Drook Formation at Pigeon Cove, Newfoundland (C-D, respectively); E-G, early silica cementation from the Aar Member of the Dabis Formation, Aus, Namibia. The fossils are *Dickinsonia costata* (A-B), cf. *Ivesheadia lobata* (C), *Trepassia wardae* (D), and *Ernietta plateauensis* (E-G). Thin sections and fossils in Condon Collection, Museum of Natural and Cultural History, University of Oregon: F1179737 (A), F117936A (B), F1179332 (C), F117935 (D), F113782 (E), F113781 (F), F113779 (G).

like those shown in here (Fig. 5I-P, Fig. 6E-F). Also fruitless were other searches for pseudomorph remnants of pyritization in classic Australian red-bed Ediacaran fossils by Gehling (1999), Mapstone and McIlroy (2006), Tarhan et al. (2015), and Retallack and Broz (2020a). Although Liu et al. (2019a, 2019b) found framboid shaped iron oxides in the Ediacara Member of South Australia, Tarhan et al. (2019) reject a "pyritic death mask" interpretation because all known framboids are too few and too dispersed to form a mask, and also not clearly associated with the fossils.

Evidence for Ediacaran oxidation during deposition of the Ediacara Member, Arumbera Formation, Grant Bluff Formation, and Maihar Sandstone comes from core and outcrop observations of unoxidized pyritic beds, as well as distinct red beds, and claystone breccias with both red-hematite and gray-pyritic clasts derived from erosion of coexisting red and gray beds (Mawson and Segnit, 1949; McMahon et al., 2020; Retallack and Broz, 2020a; Retallack et al., 2021). Loose packing of ferruginized sand grains in silica cements is also evidence for oxidation and cementation before burial compaction (Tarhan et al., 2016). Quaternary age was demonstrated for some iron oxides in the outcropping Ediacara Member by $^{234}U/^{238}U$ methods, but that isotopic system cannot return an Ediacaran age (Tarhan et al., 2018). Fresh drillcore from Ediacara DDH3 and DDH4 shows no pyrite or jarosite where cored within the Ediacara Member at 61–70 m and 58–93 m below the surface, respectively (Retallack, 2012), nor in Arumbera Sandstone red beds of Central Australia at 615–618 m in Lake Amadeus

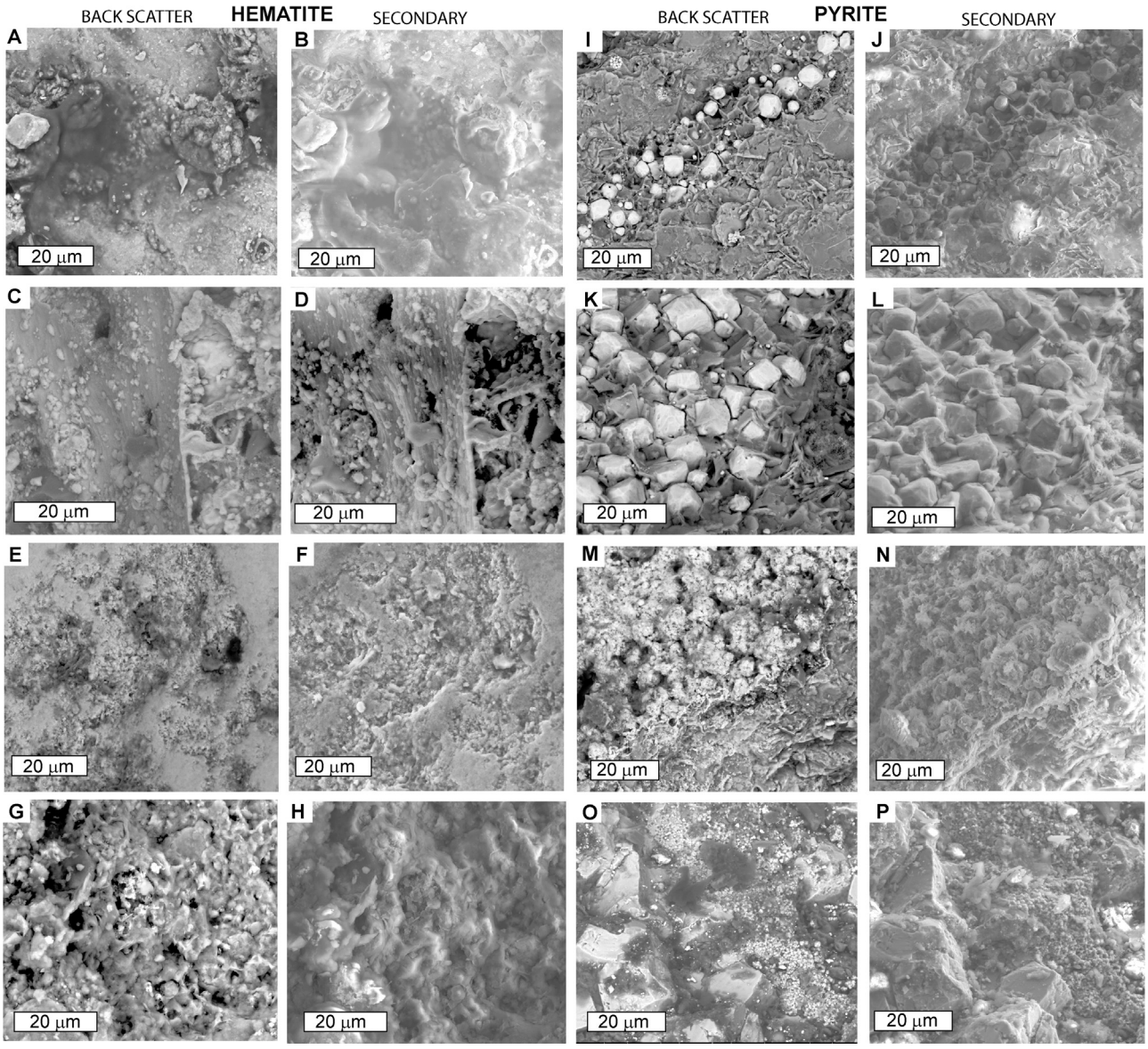

Fig. 5. Backscatter and secondary scanning electron micrographs of fossils preserved in hematite (A-H), including some oxidized from pyrite (E-F), compared with fossils preserved in pyrite (I-P); A-B, vendobiont (*Dickinsonia costata*) from the Ediacaran, Ediacara Member of the Rawnsley Quartzite in Brachina Gorge, South Australia; C - D, sandy matrix to right of leaf (*Araliopsoides cretacea*) from the Cretaceous (Cenomanian), Dakota Sandstone, near Hoisington Kansas; E - F, ferruginized ammonite (*Myloceras joffrei*) from the Cretaceous (Albian) Wangarlu Mudstone of Harneys Beach, Northern Territory, Australia; G-H, trilobitomorph (*Naraoia spinosa*) from Cambrian (Atdabanian) Yuanshan Member, Qiogzhusi Formation of Maotianshan Hill, near Chengjiang, China; K-L, bacterial filament and trilobite (*Parabolina spinulosa*) from Cambrian (Jiangshanian), Dolgellau Member, Cwmshegen Formation, Brin-Llin-Fawr, Wales; M – N, crinoid (*Lasiocrinus scoparium*) from Devonian (Givetian), Marcellus Shale, Falling Water, West Virginia; O-P, brachiopod (*Paraspirifer brownockeri*) from Devonian (Givetian), Silica Shale, Sylvania, Ohio. Specimens in Museum of Natural and Cultural History of the University of Oregon are F34287 (A – B), F111084A (C - D), F117299 (E – F), F112961 (G – H), F109875 (I - L), F114671 (M – N), F114846 (O – P).

5 DDH01 core (Mapstone and McIlroy, 2006). Deep weathering did not oxidize outcropping pyritic black shales of the nearby Wonoka Formation and Parara Limestone, which underlie and overlie Ediacaran fossiliferous red sandstones for hundreds of kilometers along strike in dipping sequences of South Australia (Clarke, 1990; Hurtgen et al., 2005). Detailed geochemical and mineralogical study of South Australian Ediacaran rocks are unlike deep weathering profiles, either Phanerozoic (Retallack, 2010) or Ediacaran (Liivamägi et al., 2014, 2015). Ediacaran fossils of South Australia and their matrix are not kaolinite, alunite, or boehmite, but ferruginized illites with sharp 10 Å peaks in x-ray diffractograms, as evidence of late diagenetic alteration during deep burial (Retallack, 2008, 2012).

3.2. Phanerozoic ferruginization

Goethite and other iron oxyhydroxides form a death mask of minerals which do not penetrate the body. These biofilms are especially robust on deciduous leaves on pavement (Fig. 1A-C). Robust and detachable predepositional ferruginous biofilms are a taphonomic mode suggested by Spicer (1977), from observations of goethite encrustation of modern leaves in lakes (Fig. 1E). This mechanism explains why venation is so clear on fossil leaves in coarse-grained sandstone matrix (Dunn et al., 1997; Locatelli et al., 2017), well known in the mid-Cretaceous (Cenomanian) Dakota Formation of Kansas (Fig. 3F, Fig. 5C, D). This kind of death mask is ferruginous, in the original Latin sense of "rusty" (as in fer-

Table 1
Fossils considered and illustrated in this study.

Taxon	Age	Formation	Locality	Collection number	Figure herein
Palaeophytocrene foveolata, fruit	Eocene	Clarno Formation	Clarno, Oregon	OF109381	3I
Betulites westii, leaf	Cretaceous	Dakota Formation	Hoisington, Kansas	OF111085	6C-D
Dakotanthus cordiformis, flower	Cretaceous	Dakota Formation	Hoisington, Kansas	UF3428	3G
Araliopsoides cretacea, leaf	Cretaceous	Dakota Formation	Hoisington, Kansas	PB17535	3F, 5C-D
Mortoniceras inflatum, ammonite	Cretaceous	Wangarlu Mudstone	Harneys Beach, N. Territory	OF117298	6F
Myloceras joffrei, ammonite	Cretaceous	Wangarlu Mudstone	Harneys Beach, N. Territory	OF117299	3D, 5E-F
Pullisylvanoxylon arizonicum, wood	Triassic	Chinle Formation	Holbrook, Arizona	OF111197	3J
Lasiocrinus scoparius, crinoid	Devonian	Marcellus Shale	Falling Waters, West Virginia	OF114671	5M–N
Paraspirifer brownockeri, brachiopod	Devonian	Silica Shale	Toledo, Ohio	OF114846	3C, 5O-P
Langoxylon asterochlaenoideum, wood	Devonian	Bois de Bordeaux Form.	Ronquiéres, Belgium	RF107303	3B
Parabolina spinosa, trilobite	Cambrian	Cwmshegen Formation	Bryn-Llin-Fawr, Wales	OF109875	5K-L, 6E
Naraoia spinosa, trilobitomorph	Cambrian	Qiongzhusi Formation	Maotianshan, China	OF112961	5G-H
Ernietta plateauensis, vendobiont	Ediacaran	Kuibis Formation	Aus, Namibia	OF113777	3H, 4E-G
Dickinsonia costata, vendobiont	Ediacaran	Ediacara Member. Rawnsley Quartzite	Brachina Gorge, South Australia	OF34287; OF115737; F1179737 F117936A	3E, 4A-B, 5A-B, 6A-B
Ivesheadia lobate, vendobiont	Ediacaran	Drook Formation	Drook, Newfoundland	Field photo	3A, 4C
Trepassia wardae, vendobiont	Ediacaran	Mistaken Point Form.	St Schotts, Newfoundland	F117935	4D

Note: Specimen numbers are from the Institute Royal des Sciences Naturelles in Brussels (RF-), Florida Natural History Museum in Gainesville (FF-), Condon Collection of the University of Oregon Museum of Natural and Cultural History (OF-), and Thomas Burke Memorial Museum of the University of Washington in Seattle (PB-),

ruginous metal prints) or "rust colored" (as in ferruginous hawk). The term ferruginous ocean (Canfield et al., 2007) in contrast, is a misnomer, because those oceans had mainly ferrous (green) not ferric (red) iron. The red color of fossiliferous Psamment paleosols (Fig. 1H) yielding these distinctive fossils comes from ferric (Fe^{3+}) iron oxides and hydroxides. The Cretaceous fossil leaves include thin water-lily leaves, thick densely veined leaves (Fig. 3F), and woody reproductive structures (Fig. 3G). The differential relief of the fossils are not due to the ferruginous biofilm. Clay crystallinity and stratigraphic considerations indicate only 800 m of burial of these Cretaceous leaves (Retallack and Dilcher, 2012), but resistance to burial compaction was conferred in proportion to original lignin, rather than thickness of ferruginous death masks (compare Fig. 3F and G). Burial dehydration of original ferric oxides and hydroxides converted them to hematite (Retallack and Dilcher, 2012). Scanning electron microscope study of leaves from the Dakota Formation of Kansas revealed a striking difference between the biofilmed fossil and the sandy matrix (Fig. 5C-D). In electron microscope back-scatter views these hematite surfaces are gray and lack the white spheres or pyritohedra of pyritized fossils (Fig. 5C, Fig. 6C). In electron microscope secondary view, the hematite has a nearly smooth texture with microlineation like the felt of hats, and lacks spheres or pyritohedra (Fig. 5D, Fig. 6D). Other fossil leaves preserved by ferruginous biofilms in sandstone are Permian *Evolsonia* (Mamay, 1989), and Triassic *Sanmiguelia* (Tidwell et al., 1977).

In contrast with the coccoid-vibrio shape of corrosive-replacive, sulfate-reducing bacteria are filamentous biofilm-forming, iron-oxidizing bacteria (Fig. 2C-D), which form death masks, 2–3 μm thick, of ferric hydroxides on leaves in shallow lakes and puddles (Fig. 5A-C, E). Spicer (1977) found that these biofilms were created by the iron-oxidizing bacterium *Sphaerotilus natans*. These beta proteobacteria settle on surfaces by entanglement and by an adhesive base (Pellegrin et al., 1999). *Sphaerotilus*, and the similar *Leptothrix ochracea* are heterotrophic, and fueled by simple organic compounds from leaf decay (van Veen et al., 1978). Iron is not essential to the heterotrophic metabolism of *Sphaerotilus* and *Leptothrix*, and iron hydroxide biofilms may be byproducts of catalytic proteins in their mucopolysaccaride sheaths (Chan et al., 2009; Furutani et al., 2011). Iron oxyhydrates dehydrate on burial to hematite (Retallack, 1991; Mapstone and McIlroy, 2006). Filamentous iron-oxidizing bacteria with adhesive bases reproduce to form robust biofilms. Comparable filamentous iron-oxidizing bacteria have a fossil record extending back perhaps 2 billion years (Trewin and Knoll, 1999).

Ferruginous biofilms can be distinguished from pyritic fossils that have been subsequently oxidized in outcrop. Reddened but originally pyritic Cambrian fossils in yellow matrix from Chengjiang, China, are best known from the locality Maotianshan, which means "red cap hill". This name refers to laterite of Neogene age above the fossiliferous yellow beds, which are deeply weathered in the saprolite of that thick paleosol (Hou et al., 2008). The same stratigraphic level elsewhere in Yunnan has comparable pyritized fossils in black shale (Gaines et al., 2008). Oxidized trilobitomorphs from Chengjiang maintain preservation of the finest genal caecae and other internal organs in hematite spheres after framboids, and one cluster of hematite spheres includes skeletal pyrite remnant visible in back-scatter view (Fig. 5G–H). Comparable oxidation of trilobites also is found at Emu Bay, South Australia, where the fossiliferous gray shale is reddened at the lower fringe of a lateritic saprolite (Daily et al., 1974), and hematite replacing pyrite has preserved fine details of limbs, hairs, and eyes (Gabbott et al., 2004; Gaines et al., 2008; Paterson et al., 2011). Hematite ammonites (Fig. 3D) from near Darwin, Northern Territory, Australia, are found mainly loose on the beach, eroded from a nearby, thick, red laterite. This Neogene, deeply weathered, lateritic paleosol is developed on Cretaceous, Wangarlu Mudstone, which is gray and pyritic in deep drill holes (Henderson, 1990). The lateritized ammonites are very strongly ferruginized, but still betray original pyritization in the form of pitting within the original shell from former pyrite framboids (Fig. 5E–F, Fig. 6F). The overall shape of the shell interior and of septae are little disrupted by this deep pitting (Fig. 4F). Oxidized leaves with casts of framboids from Permian siltstones of abandoned paleochannels of Texas have both red hematite and yellow jarosite framboid pseudomorphs, but clear tracheids, stomates and other cells (Chaney et al., 2009).

In addition to ferruginous biofilms and oxidation of pyrite, MacGabhann et al. (2019) propose a third mechanism of Tafilalt-style preservation of problematic fossils from Ordovician rocks of Morocco: adsorption of ferrous iron on biopolymers then later oxidized to ferric iron on exposure. This particular mechanism does not explain observations made here because close examination of

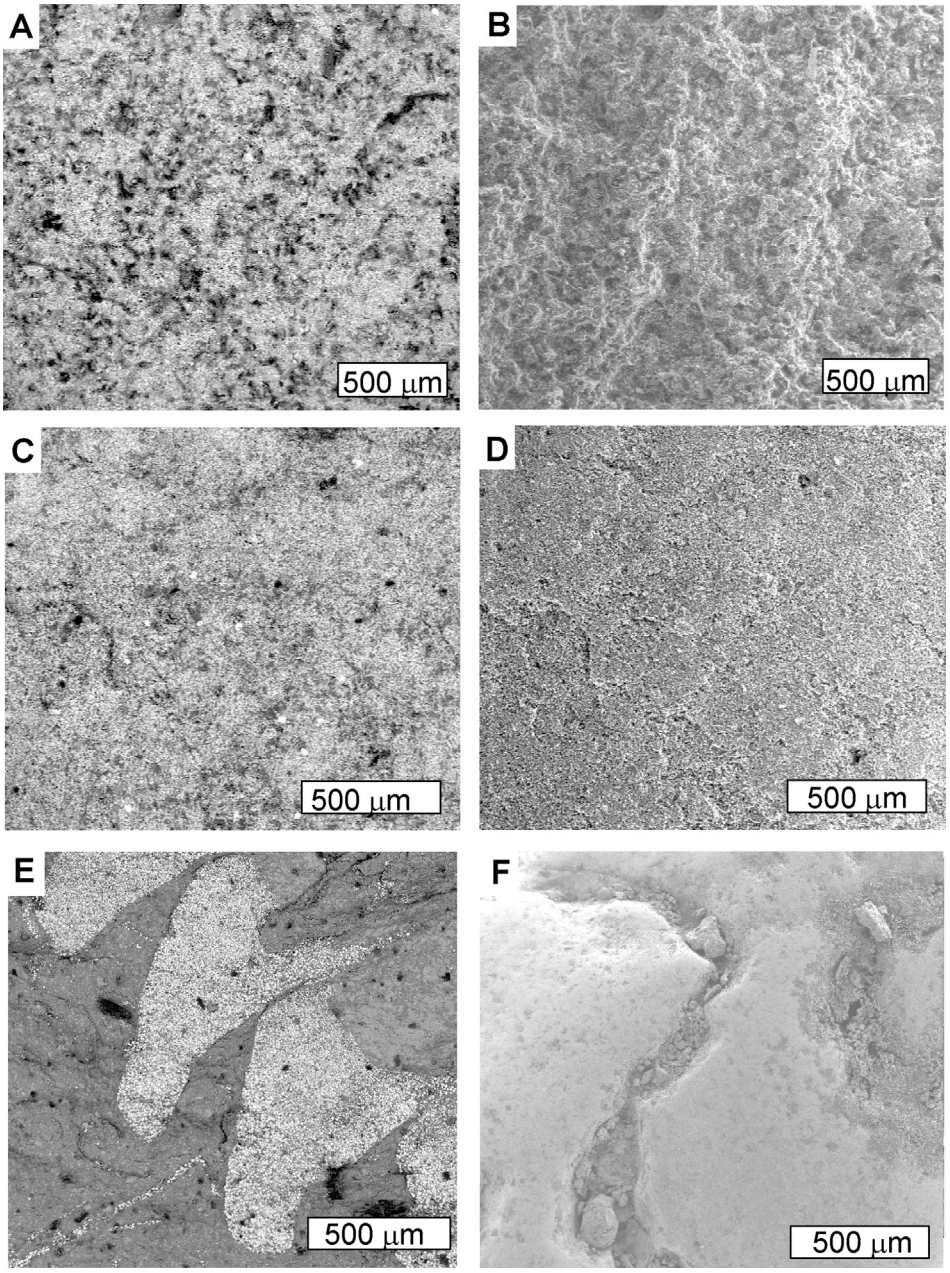

Fig. 6. Backscatter (A,C,E) and secondary electron images (B,D,F) of same small areas of *Dickinsonia costata* (A-B) from the Ediacaran, Ediacara Member of the Rawnsley Quartzite in Brachina Gorge, South Australia, and *Betulites westii* (C-D) from the Cenomanian, Dakota Sandstone, near Hoisington Kansas. No pyrite, nor casts of framboids, nor cubic crystals, were found on these ferruginous clayey surfaces. In contrast, are clear pyritohedra in a back-scatter image (E) of pleural segments of a trilobite (*Parabolina spinosa*) from the Late Cambrian (Jiangshanian) Dolgellau Member, Cwmshegen Formation of Brin-Llin-Fawr, Wales, and cavities after framboids in a secondary electron images (F) of a ferruginized ammonite (*Mortoniceras inflatum*) from the Early Cretaceous (late Albian) Wangarlu Mudstone of Harneys Beach, Northern Territory, Australia. Specimens in Museum of Natural and Cultural History of the University of Oregon are F115737 (A – B), F111085B (C - D), F109875B (E) and F117298 (F).

Ediacaran vendobionts does not reveal cell structure of original biopolymers (Fig. 5A-B, Fig. 6A-B), nor well preserved ferruginized internal structures (Fig. 4A-B). The Ediacaran oxidized iron enrichment in the Flinders Ranges of South Australia is largely at the top and bottom (Fig. 4A-B). Tafilalet-style preservation may be a case of internal pyritization, also documented in Ediacaran fossils from Mistaken Point, Newfoundland (Fig. 4C-D).

3.3. Uniquely Ediacaran ferruginization?

Hematite encrustations of Ediacaran fossils in sandstone (Fig. 3E) are no different from those of Cretaceous leaves in sandstone (Fig. 3F), and show similar microfabric (Fig. 4B, 5A-B, 6A-B). Hematite death masks of ferruginized Ediacaran fossils may have been formed by iron-oxidizing bacteria such as *Leptothrix* (Fig. 2C-D) and *Sphaerotilus*, as demonstrated for modern leaf fossils (Spicer, 1977). By this interpretation there is no evidence for chemically unique Ediacaran oceans or microbial mats required for this kind of preservation (Canfield et al., 2007; Gehling, 1999; Tarhan et al., 2016). Pyritic death masks, or solid external-only coatings of pyrite, remain to be demonstrated in any geological period.

Nor is there indication in the form of framboidal or cubic cavities that Ediacaran fossils of South and central Australia were once pyritized, but later oxidized in outcrop (Gehling, 1999; Mapstone and McIlroy, 2006; Retallack, 2014, 2016b, 2016c; Tarhan et al.,

2015, 2018, 2019). Oxidation of pyrite in saprolites of modern soils is known to be thorough at the transition from grey bedrock and saprock below the water table to yellow and mottled saprolite above (Anderson et al., 2002; Girard et al., 1997). The crystal form of pyrite weathered initially to goethite and hematite is preserved within saprolites as thick as 25 m., but becomes unrecognizable higher in soil profiles by replacement with clay and its deformation by soil structure (Girard et al., 1997). Faithful replicas of pyrite framboids in goethite are found in the mottled, intermittently drained portions of upper intertidal and surpratidal soils of Great Sippewissett Marsh (Cape Cod, Massachusetts), Sapelo Island (Georgia), and Hackensack Meadowlands (New Jersey: Luther et al., 1982). Abiotic oxidation of pyrite is complex and involves several intermediates (Luther, 1987; Moses et al., 1987), but can proceed at very low oxygen tensions by exchange with dissolved Fe^{3+} (Rimstidt and Vaughan, 2003). The rate of oxidation of pyrite is markedly accelerated by acidophilic, chemoautotrophic, iron-oxidizing bacteria, such as *Acidilithiobacillus ferrooxidans*, and *Ferrobacillus ferrooxidans*, and related species (Silverman, 1967), again within a wide range of oxygen tensions (Gleisner et al., 2006; Silverman, 1967).

4. Pyritization

4.1. Ediacaran pyritization

Ediacaran fossils from Newfoundland (Fig. 3A, 4C-D) demonstrate three degrees of pyritization: (1) complete pyritic permineralization (*Charniodiscus*, *Ivesheadia*: Retallack 2016b, 2016c), (2) unpyritized organic preservation (*Charnia*: Retallack, 2016b), or (3) mixed pyrite-organic preservation (*Aspidella*: Gehling et al., 2000: Retallack, 2016b). Regardless of degree of pyritization, all these fossils are compaction-resistant (up to 6 mm thick, not flattened like other soft-bodied fossils on the same slabs), indicating that biopolymers rather than pyrite are giving them strength to resist burial compaction (Retallack, 1994). *Ivesheadia* from Newfoundland (Fig. 3A) has an indistinct nodule-like form, and this appearance may be partly due to decay (Liu et al., 2011).

A comparable range from weak to strong pyritization has been recorded in compaction-resistant fossils of the White Sea Group of Russia (Dzik and Ivantsov, 2002; Steiner and Reitner, 2001), Khatyspyt Formation of Siberia (Bykova et al., 2017), "Mohyliv" (Mogilev) Formation of Ukraine (Dzik and Martyshyn 2015), and Dengying Formation of China (Cao et al., 2010). Some Russian pyritized fossils are replaced from within by pyrite (Steiner and Reitner, 2001), and in one case a thoroughly pyritized fossil is overgrown with a rounded and lumpy pyrite nodule that obscures its morphology rather than forming a death mask (Dzik and Ivantsov, 2002). There is some wall and internal organ pyritization, but limited lumen or matrix pyritization of Ediacaran tubular fossils from China (Cai et al., 2010), and USA (Schiffbauer et al., 2020: Smith et al., 2016). Thus no one has yet documented a pyritic "death mask" in the sense originally proposed by Gehling (1999) as a compaction-resistant, mm-thick encrustation that does not also permeate the body of a fossil. The excuse that museum curators do not allow cutting of precious specimens (Liu et al., 2019) is inadequate in view of numerous Ediacaran fossils now examined in thin and polished sections, which fail to demonstrate death masks (Dzik and Ivantsov, 2002; Gehling, 1999; Liu, 2016; Liu et al., 2019; Mapstone and McIlroy 2006; Retallack, 2016b, 2016c; Tarhan et al., 2019).

Russian and Chinese pyritic fossils are regarded as shallow marine, deltaic and estuarine, including intertidal (Bobkov et al., 2019; Bristow et al., 2009; Bykova et al., 2017; Grazhdankin, 2004). Although the Mistaken Point and Drook Formations of Newfoundland with pyritized fossils have been interpreted as deep water turbidites on basaltic oceanic crust (Ichaso et al., 2007; Wood et al., 2003), there are reasons to doubt that setting. These formations overlie a continental-margin, subduction-complex, including Holyrood Granite (Retallack, 2014). The 365 Ma age of the Mistaken Point Formation (Matthews et al., 2020) is the same as the Bou Azzer Glaciation of Morocco (Linnemann et al., 2018), and a sea-level low-stand 600 m lower than before or after in Wonoka Paleocanyons of South Australia (Retallack et al., 2014). Reexamination of the Newfoundland sequence demonstrates interbedded gray pyritic and red hematitic beds, as well as volcanic ash with gas-escape structures, and matrix-supported lapilli and crystals which could not have been deposited in any depth of water (Retallack, 2014; Retallack, 2016a). Each of these Ediacaran formations also has very low boron content typical of freshwater paleoenvironments (Retallack, 2020). A complete sulfur cycle including oxidation and reduction is known from sulfur isotopic studies of Ediacaran and geologically older pyrite and sulfate, assumed to be marine (Canfield et al., 2007; Bykova et al., 2017; Lyons et al., 2014). Low values of highly reactive iron over total iron are evidence of pyritization under near-oxic conditions in the Mistaken Point Formation of Newfoundland (Canfield et al., 2007). Such conditions are common in tidal flats and coastal plains where there is a strong gradient between air with oxygen and oxygen-depleted pore water below (Retallack, 2016c).

4.2. Phanerozoic pyritization

Pyritization can be both a form of permineralization and replacement (Schopf, 1975; Retallack, 2011, 2015, 2016b, 2016c), because organic or skeletal material of a fossil is both supported by cavity-infill, and replaced by framboidal pyrite (Fig. 3A-G, 4C-D). Plant pyritization fills cell lumens and can preserve cell walls for anatomical study, such as the complex structure of cladoxyl steles (Fig. 3B). Massively pyritized shells like those of *Paraspirifer brownockeri* retain unencrusted outer surfaces (Fig. 3C). A characteristic form of pyrite are tiny spherical framboids, often aggregated into larger spheres (Fig. 5M - P). Microscopic angular pyritohedra also are common (Fig. 5I - J), and in some cases these are visble to the unassisted eye (Fig. 5O - P), perhaps due to neomorphic growth during deep burial diagenesis (Perkins, 1998).

Pyritization is remarkable for keeping within bounds of organic structures, and continuous form-fitting external-only rinds of pyrite ("death masks") have not been found in Phanerozoic fossils. Pyritohedra are contained within tiny filaments only 18 μm wide (Fig. 5I - J), as small as sulfur bacteria such as *Beggiatoa* (Larkin and Strohl, 1983). Pleural spines of trilobites are infiltrated by pyritohedra (Fig. 6E). Gills, walking legs, antennae and other fine appendages of trilobites are faithfully replicated by pyrite, rather than obscured by encrustation (Farrell et al., 2009; Struve, 1985). Excess pyrite can form encrusting nodules that overgrow the fossil, and are partly recrystallized diagenetically from the original framboidal microstructure, but only after the inside of the fossil is thoroughly pyritized (Fisher, 1986; Marynowski et al., 2007; Matten, 1973). Phanerozoic plants and molluscs are pyritized by formation of framboids in cell lumens or within shells to create permineralized plant cells (Allison, 1988; Borkow and Babcock, 2003; Matten, 1973) or replaced and nodularized shells (Fisher, 1986; Marynowski et al., 2007).

Pyritic salt-marsh paleosols are a common location for pyritized fossils (Fig. 1D), and have a long fossil record extending back to the Cambrian (Retallack, 2013a) and Ediacaran (Retallack, 2014, 2016b-c). Unpyritized paleosols in contrast, have moldic or permineralized plant preservation (Fig. 1F, H-I). Pyritization is also known from marine anoxic basins (Fisher, 1986), but pyritization is most intense within the modern intertidal zone

(Clark and Lutz, 1980; Thomas et al., 2004). Sea water delivers abundant sulfate, and organic soils of salt marsh grasses and mangroves with high water tables provide an anaerobic environment for the activity of sulfate-reducing bacteria, such as *Desulfovibrio* (Altschuler et al., 1983). The corrosive and replacive nature of sulfate-reducing bacteria can be related to their formation of sulfuric acid intermediaries and coccoid to short vibrio morphology (Fig. 2A-B). The short curved-rod form of *Desulfovibrio* (Gilmour et al., 2011) contrasts with the coccoid form of other sulfate-reducing microbes (Thauer et al., 2007). Other mesophilic sulfate-reducing delta proteobacteria include *Desulfobacterium*, *Desulfobacter*, and *Desulfobulbus*. The four other sulfate-reducing lineages are also anaerobic, but thermophilic: (1) gram negative bacteria such as *Thermodesulfovibrio*, (2) Gram positive bacteria such as *Desulfotomaculum*, (3) clostridian bacteria such as *Thermodesulfobium*, and (4) Euryarchaeota such as *Archaeoglobus* (Thauer et al., 2007). Curved rods of *Desulfovibrio* are common within invasive metal corrosion (Fig. 2A; Dinh et al., 2004). Both the energy and carbon source for sulfate-reducing bacteria are organic compounds (Birnbaum and Wireman, 1984). This explains the common geological association of pyrite with organic-rich black shales (Borkow and Babcock, 2003; Fisher, 1986). Sulfate in sea water is the electron acceptor used to create biogenic pyrite (mainly framboids) under anaerobic conditions (Voordouw, 1995). Comparable bacteria can be inferred back well before the Ediacaran by isotopic fractionations of sulfur in pyrite compared with sulfate (Hurtgen et al., 2005).

4.3. Uniquely Ediacaran pyritization?

Liu (2016) argues "that in the Phanerozoic, pyritization is usually spatially restricted to only the area immediately surrounding organisms, and is typically documented in fine-grained clastic successions, whereas in the Ediacaran, pyritization often extends across entire bedding surfaces, in a range of different lithologies." This observation neglects extensive pyritic layers and nodules in intertidal paleosols and soils on mud, sand, and limestone, under salt marsh, mangroves, and other intertidal vegetation of Ediacaran to Holocene age (Fig. 1D,G). Such Phanerozoic intertidal pyritic nodular paleosols are common and widespread (Altschuler et al., 1983; Clark and Lutz, 1980; Retallack, 2013a, 2015, 2016c; Retallack and Dilcher, 2012; Retallack and Kirby, 2007). Ediacaran intertidal pyritic paleosols also have extensive nodules and layers of pyrite (Retallack, 2014, 2016b, 2016c), much more heavily pyritized than surface Ediacaran biofilms (Steiner & Reitner, 2001).Precision Ediacaran pyritization of guts (Schiffbauer et al., 2020) and hyphae (Gan et al., 2021), is matched by equally precise pyritization of trilobite antennae, guts and gills (Struve, 1985; Farrell et al., 2009). Because Ediacaran intertidal pyritic preservation is not discernably different from Phanerozoic intertidal pyritization (Clark and Lutz 1980; Altschuler et al., 1983; Retallack and Dilcher, 2012; Retallack and Kirby, 2007), there is no evidence for a taphonomic window of uniquely Ediacaran pyritic "death masks" closed by advent of Cambrian marine bioturbation (Gehling, 1999), or changes in marine chemistry (Canfield et al., 2007, 2010).

Laboratory experiments with chitinous exoskeletons of arthropods reveal formation of ellipsoidal nodules of pyrite rather than thin pyritic rinds (Darroch et al., 2012). These forms of interior replacement followed by overgrowing nodularization are similar to pyritization observed throughout the fossil record (Allison, 1988; Fisher, 1986; Marynowski et al., 2007; Matten, 1973), and reflect the dependence of sulfate-reducing bacteria on organic substrates.

5. Silica and phosphate permineralization

5.1. Ediacaran silica and phosphate permineralization

The most biologically informative mode of fossil preservation is silica permineralization, which is known in Ediacaran megafossils and microfossils (Fig. 7). Silica permineralization of Ediacaran microfossils have organic cell walls remaining, but supported outside and inside with transparent colloidal silica (Liu et al., 2014; Xiao, 2004; Xiao et al., 2010). Millimetric fossils of *Horodyskia* and *Palaeopascichnus* have also been found silicified (Dong et al., 2008). In another Ediacaran example, microscopic, pyritized, fungal hyhae are embedded in chalcedony (Gan et al., 2021). Ediacaran phosphate permineralised microfossils are also known (Chen et al., 2009; Xiao et al., 2014), including remains interpreted at first as embryos, but subsequently as mesomycetozoa (Huldtgren et al., 2011). Millimetric fragments of phosphatized Ediacaran thall, identified as glomeromycotan or mucoromycotan lichens, have filamentous structure with terminal vesicles (Yuan et al., 2005). Large silica-permineralized fossils (8 × 12 cm) of *Petalostroma kuibis* from Namibia (Pflug, 1973, 1994) have an internal histology of long tubular cells, and spheroidal cells with haustorial hyphal dimples (Fig. 7). These tubular cells and spheroids form the margin of larger tubes (Fig. 7A), and spheres with budding tubes (Fig. 7B). The beauty of such preservation is its unexpected biological detail: the tubular cells have been interpreted as aseptate fungal hyphae, the spheroids as endosymbiotic cyanobacteria, the larger tubes as fungal podetia, and the large spheres with budding tubes as fungal isidia (Retallack, 1994). In both phosphatization and silicification, colloidal mineral fills cell lumens and preserves microscopic details unobtainable in other forms of preservation.

Examination of thin sections of *Ernietta plateauensis* did not reveal such details (Retallack, 2016b; Elliott et al., 2016; Ivantsov et al., 2016), as perhaps could have been predicted from their reddish tinge of hematite, an indication of oxidation of much organic matter (Fig. 3K). The best-preserved silica permineralized fossils are distinguished by black to dark brown color and soft tissue preservation (Gould and Delevoryas 1977; Gould, 1971; Nishida et al., 2004). Although the interior of Ediacaran *Ernietta* from Namibia is filled with sand, it is cemented with silica cement predating burial compation (Fig. 4E - G). Similarly, *Dickinsonia* specimens are simple films between two beds of sandstone (Retallack, 2007), but some specimens show silica cementation of a thick body with a distinct orthogonal network of wall layers (Fig. 4A – B). The preserved biological structures are not always as clear as in unoxidized silicified fossils, but consistent from specimen to specimen in showing opaque partitions of less opaque regions (pneu structure of Seilacher, 1989). These orthogonal internal partitions are evidence that *Dickinsonia* is not preserved as rheid deformation into cavities, as proposed by Wade (1968) and Bobrovskiy et al. (2019). Nor was it necessarily a wormlike creature, inferred from isolation of cholesterol from *Dickinsonia* (Bobrovksiy et al., 2018), because cholesterol is also known in many fungi and red algae (Retallack, 2020). The preservation of South Australian moldic *Dickinsonia* (Fig. 3E) and other vendobionts is most like preservation of leaves in sandstone poor in organic matter (Fig. 3F: Retallack and Dilcher 2012). The moldic preservation of Nambian *Ernietta* (Fig. 3H) is most like plants such as *Stigmaria* and *Calamites* in Pennsylvanian quartz sandstones (ganisters: Retallack, 1977; Percival, 1983).

Early diagenetic silica cements of vendobionts have also been recently demonstrated by cement-supported, uncompacted grains within hollow holdfasts of Ediacaran frond fossils from Nilpena, South Australia (Tarhan et al., 2016) and experimental studies (Slagter et al., 2020). Median Ge/Si values 2.51 μmol/mol (but up

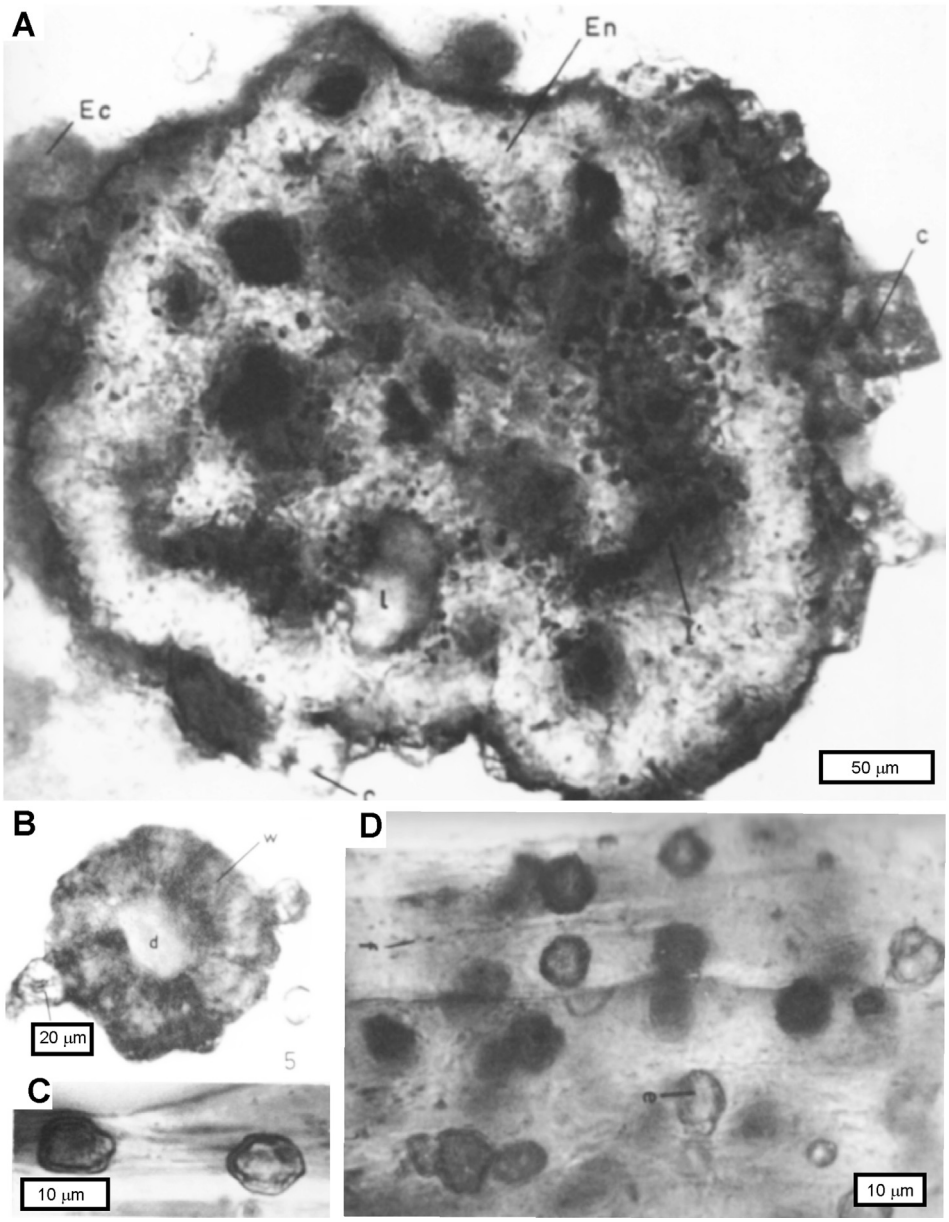

Fig. 7. Petrographic thin sections of *Petalostroma kuibis* (from Pflug, 1973), upper Kliphoek Formation of the Dabis Formation (late Ediacaran) at Aarhausen locality, Namibia (Vickers Rich *et al.*, 2016); A, large tubule containing spheroidal cell clusters; B, spheroidal cell cluster with budding tubular cells; C, details of dimpled spheroidal cells wthin large tubular cells; D, spheroidal cells within tube-margin tubular cells. These structures may be fungal podetia (A), isidia (B), photobionts (C) and hyphae (D: Retallack, 1994). Figures from Pflug (1973) with permission from Sschweitzerbartsche.

to 10 μmol/mol) for early diagenetic cements within Ediacaran holdfasts contrast with 0.91 μmol/mol (but up to 4 μmol/mol) for clastic grains derived from granitic source terrains. The cements are pedogenic (Ge/Si > 1), not marine, nor aquatic (Kurtz et al., 2002; Street-Perrott and Barker (2008)). Archean paleosols also have high Ge/Si ratios (1.06 to 3.22 μmol/mol; Delvigne et al., 2016). Marine and fresh waters and biogenic silica in contrast have Ge/Si ratios less than 1 μmol/mol (Filippelli et al., 2000); Murray et al., 1991), as do Archean (Delvigne et al., 2012) and Ediacaran marine cherts (Dong et al., 2015; Wen et al., 2016). An exception is Ediacaran siliceous nodules with Ge/Si values as high as 2.54 μmol/mol (Shen et al., 2011) due to pedogenic saponite (Bristow et al., 2009). High Ge/Si ratios of 8–20 μmol/mol also are common in hydrothermal solutions, sinters, cherts, and iron-rich parts of banded iron formations (Mortlock et al., 1993; Delvigne et al., 2012), but there are no independent indications of hydrothermal alteration or banded iron formation with Ediacaran fossils in South Australia (Retallack, 2012; Tarhan et al., 2016).

5.2. Phanerozoic silicification and phosphatization

Permineralizing silica fills cell lumens of fossil plants, fungi, and insect carapaces (Retallack, 2011). Permineralization has been urged instead of the familiar term petrified, because original cell walls are not turned to stone, but faithfully preserved within engulfing colloidal silica (Schopf, 1975). Nevertheless, Petrified Forest National Park in Arizona is not a complete misnomer: although it has much permineralized wood, it also yields red agatized wood with poor or no cell structure, thus literally petrified or "made into stone" (Fig. 3J). The Eocene Clarno Nut beds also has both permineralized and agatized fossil fruits and seeds

(Manchester, 1994), that are also ferruginized (Fig. 3I). The red color of these fossils comes from hematite, and its oxidation in associated paleosols was accompanied by some aerobic decomposition of plant material (Sigleo, 1978, 1979; Retallack, 1997). Silica permineralization of Phanerozoic plants can give many useful biological details, such as mesenchyme lacunae and palisade structure of leaves (Fig. 8A), aerating lumens in woody roots (Fig. 8B), details of megasporophylls with ovules (Fig. 8C), and even pollen in the pollen chamber of ovules (Fig. 8D: Gould and Delevoryas, 1977). Such information is invaluable for biological understanding of fossil plants. Silica and calcite permineralization is capable of preserving very delicate biological microstructures, including sperm (Nishida et al., 2004), and nuclei (Gould, 1971). Plants are most commonly permineralized in silica, but rare remains of arthropod exoskeletons without internal soft tissue are also known (Whalley and Jarzembowski, 1981). Phanerozoic calcite permineralization can also preserve delicate structures of plants including pollen tubes (Rothwell, 1972), and fat globules (Baxter and Willhite, 1969). Phanerozoic phosphate also permineralizes soft tissues including muscle fibers (Martill, 1990), prokaryotes (Martill and Wilby (1994)), egg membranes, and embryos (Bengtson and Zhao, 1997).

Silica permineralization can grade into mold and cast preservation, in which sandstone has been cemented with silica before compaction. In fossil fruits, an internal mold of an endocarp can be called a locule cast (Manchester, 1994; Manchester et al., 2018). In plants, the difference is that the casting body is not usually a skeleton or shell, but organic matter prone to decay. Thus, red permineralized and agatized wood can pass laterally in the same specimen to log casts and stump casts where the wood has rotted away (Sigleo, 1978, 1979; Retallack 1997). An exception in plants is calcite and silica biomineralized endocarps of hackberry (*Celtis*), which are a form of plant hard part with a central hollow that may be filled with sediment or cement (Retallack, 1984). Early silica cement of fossil molds and casts is especially well seen in fossil ganisters, which are silicified eluvial horizons of paleosols (Retallack, 1977; Percival, 1983). Carboniferous equisetalean pith casts and stigmarian root casts in growth position are commonly cemented with early-diagenetic silica that fortifies them against burial compaction (Percival, 1983; Gastaldo, 1992; Retallack, 1994).

5.3. Uniquely Ediacaran permineralization?

Tarhan et al. (2016) conclude that "death and burial of Ediacara communities were followed by rapid nucleation of silica films on macroorganisms and matgrounds and precipitation in the surrounding pore space", and that "closure of the Ediacara-style preservational window may therefore reflect global scale evolution of the marine silica cycle." Their analysis assumes that Ediacaran vendobionts were marine, an assumption which has failed recent tests (Retallack, 2016b, 2020, 2022). Silica permineralization is best known from terrestrial facies, especially of fossil plants (Fig. 8). None of the observations of Tarhan et al. (2015, 2016) are unequivocally marine, and evidence from Ge/Si ratios of early diagenetic cements, from stable isotopes of calcareous nodules, wind-drift laminae, and from boron assay and geochemical mass balance (tau analysis) of substrates, supports terrestrial habitats (Retallack, 2016b, 2017, 2019, 2020). There is a continuous Phanerozoic fossil record of Ediacara-style raised impressions of fossil plants, arthropods and skin impressions in quartz sandstones (Hall et al., 1988; McNamara & Trewin, 1993; Gastaldo, 1992; Retallack, 1994; Anderson et al., 1998; Paik et al., 2010; Retallack and Dilcher 2012; Barth et al., 2013; MacGabhann et al., 2019), due to compaction-resistance of lignin and chitin, as well as early cementation (Retallack, 1994). There is no obvious difference between Ediacaran and Phanerozoic silica permineralization or silica cementation of moldic preservation.

An influential theory of wood permineralization arising from experimental work of Leo and Barghoorn (1976) is that silicic acid $[H_4Si(OH)_4]$ in aqueous solution forms hydrogen bonds with holocellulosic complexes of cell walls. Silicic acid can be elevated in hydrothermal hot springs (Rice et al., 2002), or in low temperature ground waters or formation waters by devitrification of volcanic

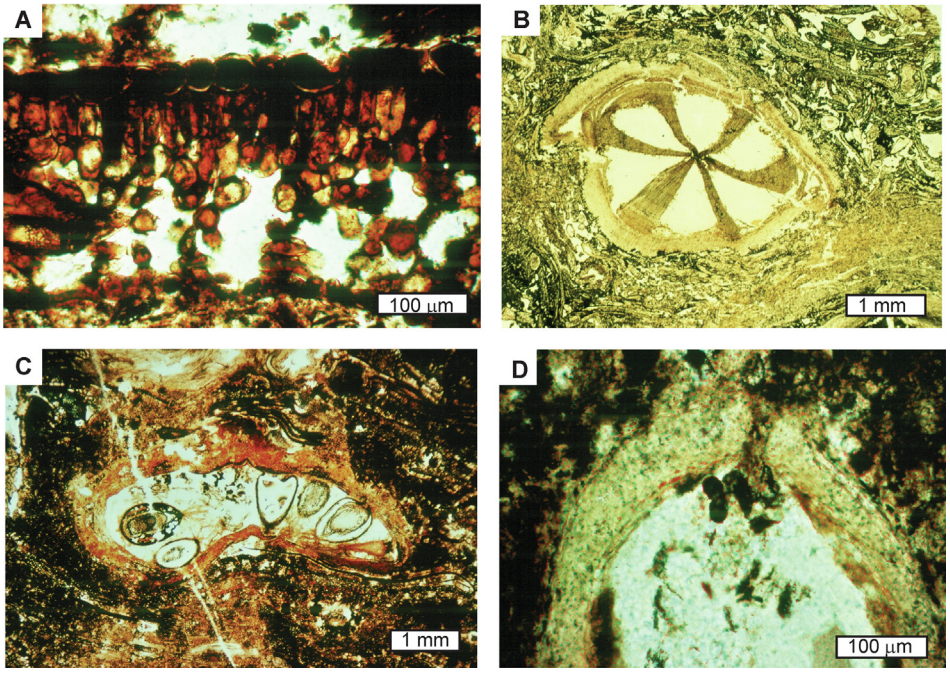

Fig. 8. Petrographic thin sections of silica permineralised remains of leaves and fertile structures attributed to *Glossopteris* from the Late Permian Fort Cooper Coal Measures near Homevale Station, Queensland (after Gould and Delevoryas, 1977); A, cross section of leaf with upper palisade, lower mesenchyme and stomatiferous lower surface; B, cross section of chambered root; C, cross section os seed-bearing structure; D, cross section of apex of ovule with pollen grains clustered in the pollen chamber.

shards (Murata, 1940), or diagenesis of clay minerals (Sigleo, 1979) and feldspars (Matysová et al., 2010). Observations of wall silicification before cell interiors in volcanic lahars of Mt St Helens support this model of precipitation from solution (Karowe and Jefferson, 1987). Subsequent experimental studies show that this can take thousands of years (Ballhaus et al., 2012), but possible accelerants include nuclei of biogenic opal (Richmond and Sussman, 2003), and silica spicules from sulfate-reducing bacteria in early stages of cytoplasmic decay (Birnbaum and Wireman, 1984, 1985).

The red to brown color of some fossil woods and Ediacaran fossils comes from occluded goethite and hematite, usually associated with fossil wood as a red paleosol or fluvial matrix (Sigleo, 1978; Matysová et al., 2010). Goethite and hematite are stable in aerobic environments, in which a variety of aerobic decomposers would have been active (Retallack, 1984, 2011), and so explain the poor preservation of cellular detail in red-brown fossil woods (Sigleo, 1978, 1979; White, 1991).

6. Conclusions

Ediacaran fossils are preserved by the same processes as Phanerozoic fossils, with the exception of freezing, mummification, amber entombment, and charcoalification (Schopf, 1975; Retallack, 2011). Preservation of the complexly-quilted, soft-bodied Ediacaran fossils known as vendobionts is most similar to that of modern and Phanerozoic fossil plants (Fig. 9), and not unique to the Ediacaran Period. Ediacaran to recent taphonomic modes include pyrite permineralization and replacement (Steiner and Reitner, 2001; Dzik and Ivantsov, 2002; Gehling et al., 2000), pyrite oxidation to hematite (Cai et al., 2010; Liu et al., 2011), silica permineralization and cementation (Pflug, 1973, 1994; Xiao 2004; Xiao et al., 2010; Liu et al., 2014; Tarhan et al., 2016), phosphate permineralization (Yuan et al., 2005; Chen et al., 2009; Xiao et al., 2014), ferruginous biofilms (Spicer, 1977), and molds and casts (Dzik, 1999; Bouougri et al., 2011). Pyritization by sulfate-reducing bacteria is penetrative and replacive (Dinh et al., 2004), but ferruginous surficial biofilms from iron-oxidizing bacteria are woven filaments with adhesive bases (Pellegrin et al. 1999; Furutani et al. 2011). Examination of numerous Ediacaran fossils in red sandstone (Figs. 3-4), and by Mapstone and McIlroy (2006) and Tarhan et al. (2019), found no evidence of uniquely Ediacaran death masks either of pyrite, nor of pyrite subsequently oxidized to hematite in outcrop (Gehling, 1999). Nor are pyritic death masks found in Phanerozoic fossils (Allison, 1988; Fisher, 1986), nor modern observations of pyritization (Clark and Lutz, 1980; Altschuler et al., 1983; Darroch et al., 2012). Pyrite replacement and nodules are strongly resistant to burial compaction (Matten, 1973; Allison, 1988), but ferruginous biofilms are thin and weak (Spicer, 1977), so that compaction-resistance of fossil leaves preserved in this way is determined by degree of original lignification (Retallack and Dilcher, 2012). Thus, observed resistance of red Ediacaran sandstone fossils to burial compaction is more likely due to an original compaction-resistant biopolymer, such as chitin, rather than the ferruginous death mask (Retallack, 1994, 2007; Fedonkin 2002). Cementation by early diagenetic silica also maintained Ediacaran fossil relief (Tarhan et al., 2016) in a process similar to preservation of stigmarian root traces in ganisters of paleosols (Retallack, 1977,

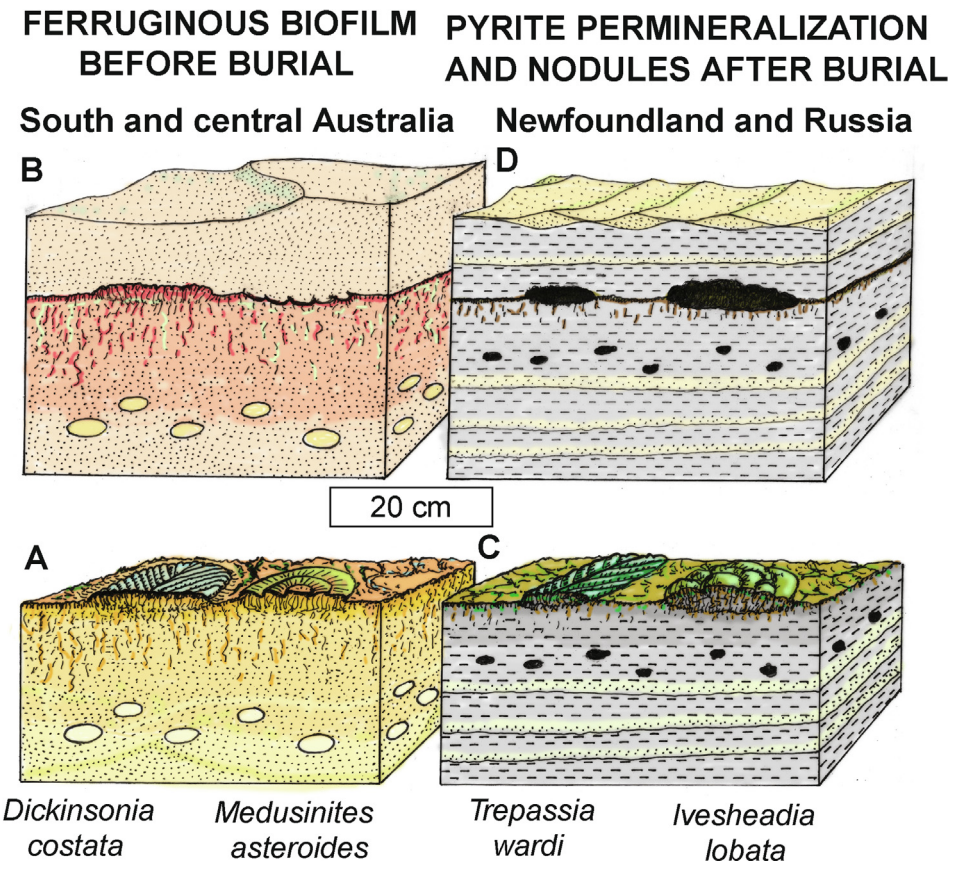

Fig. 9. Models for two common modes of microbial preservation of unskeletonized Ediacaran fossils. A-B, ferruginous biofilms transform to hematite during burial from iron oxyhydrates precipitated by aerobic iron-oxidizing bacteria consuming organic matter of the fossil shortly after death. C-D, pyrite permineralization forms by burial and precipitation by anoxic sulfate reducing bacteria consuming organic matter. A-B, based on observations in the Ediacara Member in Brachina Gorge, South Australia (Retallack, 2013b), and C-D, based on observations in the Drook Formation at Pigeon Cove, Newfoundland (Retallack, 2014, 2016b-c).

2016b; Percival, 1983). Ferruginous biofilms nevertheless enhance detail visible on Ediacaran (Retallack, 2007), Permian (Mamay, 1989), Triassic (Tidwell et al., 1977), and Cretaceous (Retallack and Dilcher, 2012) fossils in sandstone. Silica permineralized Ediacaran fossils (Pflug, 1973, 1994; Xiao, 2004; Xiao et al., 2010; Liu et al., 2014) appear preserved in ways comparable with permineralized fossil wood and seeds (Manchester, 1994; Wright, 2002), but show neither plant nor animal histology (Retallack, 1994, 2016b). Molds and casts can also be very resistant to burial compaction if formed from quartz sandstone (Dzik, 1999). A summary of two common Ediacaran modes of preservation of ferruginous biofilm and pyrite permineralization comparable with Phanerozoic plant preservation are shown in Fig. 9.

The "pyritic death mask" concept of Gehling (1999) is an example of several hypotheses which abandon the present as a guide to interpreting Ediacaran preservational and living paleoenvironments. For example, soft-bodied Ediacaran fossils have been considered preserved in a world with ineffective decomposers (Seilacher, 1989). Ediacaran fossils have been considered to lack modern analogues, and extinguished with the rise of bioturbation at the base of the Cambrian (Seilacher, 1999). Ediacaran oceans have been argued to have the low sulfur content of Swiss lakes and unusually low highly reactive iron relative to total iron (Canfield et al., 2007). Each of these non-uniformitarian hypotheses is unlikely for the following reasons. Differential decay of Ediacaran megafossils and acritarchs is well documented (Retallack, 2007; Grey and Willman 2009; Liu et al., 2011). Some vendobiont-like fossils persisted through to the Devonian with preservational style similar to that in Ediacaran (Jensen et al., 1998; Retallack, 2009, 2015). Rocks with anomalous sulfur and reactive iron contents for marine sediments alternate within meters with normal marine values for these values (Canfield et al., 2007), and it is more likely that the anomalous beds are paleosols exposed by sea-level change than due to abrupt whole-ocean change in chemistry (Retallack, 2013b, 2014). Ediacaran paleoenvironments may have been odd and did predate the evolution of land plants and extensive marine benthic burrowing, but did not have discernably distinct styles of fossil preservation.

Declaration of Competing Interest

The author declares that he has no known competing financial interests or personal relationships that could have appeared to influence the work reported in this paper.

Acknowledgments

Thanks are due to Nathan Sheldon, Evelyn Krull, Tim Jefferson, Stuart Birnbaum, Guy Narbonne, and Nora Noffke for useful discussion. Alex Liu and Breandhán MacGabhann offered helpful reviews of earlier drafts of this work. Machine time on the scanning electron microscope was funded by a program grant from the College of Arts and Sciences of the University of Oregon.

References

Allison, P.A., 1988. Taphonomy of the Eocene London Clay biota. Palaeontology 31, 1079–1100.
Altschuler, Z.S., Schnepfe, M.M., Silber, C.C., Simon, E.O., 1983. Sulfur diagenesis in Everglades peat and the origin of pyrite in coal. Science 221, 221–227.
Anderson, B.G., Lucas, S.G., Barrick, R.E., Heckert, A.B., Basabilvazo, G.T., 1998. Dinosaur skin impressions and associated skeletal remains from the Upper Campanian of southwestern New Mexico: New data on the integument morphology of hadrosaurs. J. Vert. Paleont. 18 (4), 739–745.
Anderson, S.P., Dietrich, W.E., Brimhall, G.H., 2002. Weathering profiles, mass-balance analysis, and rates of solute loss: Linkages between weathering and erosion in a small, steep catchment. Geol. Soc. Amer. Bull. 114 (9), 1143–1158.
Bailey, R.H., 1987. Stratigraphy of the Boston Bay Group, Boston area, Massachusetts. In Roy, D.C. (Ed.), Centennial field guide, Northeastern Section of the Geological Society of America. Geol. Soc. America, Boulder, 5, 209–212.
Ballhaus, C., Gee, C.T., Bockrath, C., Greef, K., Mansfeldt, T., Rhede, D., 2012. The silicification of trees in volcanic ash - An experimental study. Geochim. Cosmochim. Acta 84, 62–74.
Barth, G., Nel, A., Franz, M., 2013. Two new odonate-like insect wings from the latest Norian of northern Germany. Polish J. Entomol. 82, 127–142.
Baxter, R.W., Willhite, M.R., 1969. The morphology and anatomy of Alethopteris lesquereuxii Wagner. Univ. Kansas Sci. Bull. 48, 767–783.
Becker-Kerber, B., Elmola, A.A., Zhuravlev, A., Gaucher, C., Simões, M.G., Prado, G.M. E.M., Gámez Vintaned, J.A., Fontaine, C., Lino, L.M., Ferreira Sanchez, D., Galante, D., Paim, P.S.G., Callefo, F., Kerber, G., Meunier, A., El Albani, A., 2021. Clay templates in Ediacaran vendotaeniaceans: Implications for the taphonomy of carbonaceous fossils. Geol. Soc. Amer. Bull. https://doi.org/10.1130/B36033.1.
Bengtson, S., Zhao, Y., 1997. Fossilized metazoan embryos from the earliest Cambrian. Science 277 (5332), 1645–1648.
Birnbaum, S.J., Wireman, J.W., 1984. Bacterial sulfate reduction and pH: implications for early diagenesis. Chem. Geol. 43 (1-2), 143–149.
Birnbaum, S.J., Wireman, J.W., 1985. Sulfate-reducing bacteria and silica solubility: a possible mechanism for evaporite diagenesis and silica precipitation in banded iron formations. Canad. J. Earth Sci. 22 (12), 1904–1909.
Bobkov, N.I., Kolesnikov, A.V., Maslov, A.V., Grazhdankin, D.V., 2019. The occurrence of *Dickinsonia* in non-marine facies (La aparición de *Dickinsonia* en facies no marinas). Estudios Geológicos 75, e096.
Bobrovskiy, I., Hope, J.M., Ivantsov, A., Nettersheim, B.J., Hallmann, C., Brocks, J.J., 2018. Ancient steroids establish the Ediacaran fossil *Dickinsonia* as one of the earliest animals. Science 361 (6408), 1246–1249.
Bobrovskiy, I., Krasnova, A., Ivantsov, A., Luzhnaya (Serezhnikova), E., Brocks, J.J., 2019. Simple sediment rheology explains the Ediacara biota preservation. Nature Ecol. Evol. 3 (4), 582–589.
Borkow, P.S., Babcock, L.E., 2003. Turning pyrite outside-in: the role of microbial biofilms in pyritization of fossils. The Sedimentary Record 1, 1–4.
Bouougri, E.H., Porada, H., Weber, K., Reitner, J., 2011. Sedimentology and palaeoecology of Ernietta-bearing Ediacaran deposits in Southern Namibia: Implications for infaunal vendobiont communities. In: Reitner, J., Quéric, N.V., Arp, G. (Eds.), Advances in Stromatolite Geobiology. Springer, Berlin, pp. 474–505.
Bristow, T.F., Kennedy, M.J., Derkowski, A., Droser, M.L., Jiang, G., Creaser, R.A., 2009. Mineralogical constraints on the paleoenvironments of the Ediacaran Doushantuo Formation. U.S Nat. Acad. Sci. Proc. 106 (32), 13190–13195.
Bykova, N., Grazhdankin, D.V., Rogov, V.I., Xiao, S., 2017. A geochemical study of the Ediacaran discoidal fossil *Aspidella* preserved in limestones: implications for taphonomy and paleoecology. Geobiology 15, 1–16.
Canfield, D.E., Farquhar, J., Zerkle, A.L., 2010. High isotope fractionations during sulfate reduction in a low-sulfate euxinic ocean analog. Geology 38 (5), 415–418.
Canfield, D.E., Poulton, S.W., Narbonne, G.M., 2007. Late Neoproterozoic deep-ocean oxygenation and the rise of animal life. Science 315 (5808), 92–95.
Cai, Y., Hua, H., Xiao, S., Schiffbauer, J.D., Li, P., 2010. Biostratinomy of the Late Ediacaran pyritized Gaojiashan Lagerstätte from southern Shaanxi, China: importance of event deposits. Palaios 25, 487–506.
Carney, J.N., Alexandre, P., Pringle, M.S., Pharaoh, T.C., Merriman, R.J., Kemp, S.J., 2008. ^{40}Ar–^{39}Ar isotope constraints on the age of deformation in Charnwood Forest. UK. Geol. Mag. 145 (5), 702–713.
Chan, C.S., Fakra, S.C., Edwards, D.C., Emerson, D., Banfield, J.F., 2009. Iron oxyhydroxide mineralization on microbial extracellular polysaccharides. Geochim. Cosmochim. Acta 73 (13), 3807–3818.
Chaney, D.S., Mamay, S.H., DiMichele, W.D., Kerp, H., 2009. *Auritifolia* gen. nov., probably seed plant foliage with Comioid affinitites from the Early Permian of Texas, U.S.A. Int. J. Plant Sci. 170, 247–266.
Chen, J.Y., Bottjer, D.J., Davidson, E.H., Li, G., Gao, F., Cameron, R.A., Hadfield, M.G., Xian, D.C., Tafforeau, P., Jia, Q.J., Sugiyama, H., 2009. Phase contrast synchrotron X-ray microtomography of Ediacaran (Doushantuo) metazoan microfossils: Phylogenetic diversity and evolutionary implications. Precambrian Res. 173, 191–200.
Clark, G.R., Lutz, R.A., 1980. Pyritization in the shells of living bivalves. Geology 8 (6), 268. https://doi.org/10.1130/0091-7613(1980)8<268:PITSOL>2.0.CO;2.
Clarke, J.D.A., 1990. Slope facies deposition and diagenesis of the Early Cambrian Parara Limestone, Wilkawillina Gorge, South Australia. In Jago, J.B., Moore, P.S. (eds), The evolution of a late Precambrian–early Palaeozoic rift complex: The Adelaide Geosyncline. Geol. Soc. Australia Spec. Publ. 16, 230–246.
Daily, B., Twidale, C.R., Milnes, A.R., 1974. The age of the lateritized summit surface on Kangaroo Island and adjacent areas of South Australia. Geol. Soc. Australia J. 21 (4), 387–392.
Darroch, S.A.F., Laflamme, M., Schiffbauer, J.D., Briggs, D.E.G., 2012. Experimental formation of a microbial death mask. Palaios 27 (5), 293–303.
Delvigne, C., Cardinal, D., Hofmann, A., André, L., 2012. Stratigraphic changes of Ge/Si, REE+Y and silicon isotopes as insights into the deposition of a Mesoarchaean banded iron formation. Earth Planet. Sci. Lett. 355-356, 109–118.
Delvigne, C., Opfergelt, S., Cardinal, D., Hofmann, A., André, L., 2016. Desilication in Archean weathering processes traced by silicon isotopes and Ge/Si ratios. Chem. Geol. 420, 139–147.
Dinh, H.T., Kuever, J., Mußmann, M., Hassel, A.W., Stratmann, M., Widdel, F., 2004. Iron corrosion by novel anaerobic microorganisms. Nature 427 (6977), 829–832.

Dong, Lin, Xiao, Shuhai, Shen, Bing, Zhou, Chuanming, 2008. Silicified *Horodyskia* and *Palaeopascichnus* from upper Ediacaran cherts in South China: tentative phylogenetic interpretation and implications for evolutionary stasis. J. Geol. Soc. London 165 (1), 367–378.
Dong, L., Shen, B., Lee, C.-T., Shu, X.-J., Peng, Y., Sun, Y., Tang, Z., Rong, H., Lang, X., Ma, H., Yang, F., Guo, W., 2015. Germanium/silicon of the Ediacaran-Cambrian Laobao cherts: Implications for the bedded chert formation and paleoenvironment interpretations. Geochem. Geophys. Geosyst. 16 (3), 751–763.
Dunn, K.A., McLean, R.J.C., Upchurch, G.R., Folk, R.L., 1997. Enhancement of leaf fossilization potential by bacterial biofilms. Geology 25 (12), 1119. https://doi.org/10.1130/0091-7613(1997)025<1119:EOLFPB>2.3.CO;2.
Dzik, J., 1999. Organic membranous skeleton of the Precambrian metazoans from Namibia. Geology 27 (6), 519. https://doi.org/10.1130/0091-7613(1999)027<0519:OMSOTP>2.3.CO;2.
Dzik, J., Ivantsov, A.Y., 2002. Internal anatomy of a new Precambrian dickinsoniid dipleurozoan from northern Russia. Neues Jb. Geol. Paläont. Monats. 2002 (7), 385–396.
Dzik, J., Martyshyn, A., 2015. Taphonomy of the Ediacaran *Podolimirus* and associated dipleurozoans from the Vendian of Ukraine. Precambrian Res. 269, 139–146.
Elliott, D.A., Trusler, P.W., Narbonne, G.M., Vickers-Rich, P., Morton, N., Hall, M., Hoffmann, K.H., Schneider, G.I.C., 2016. *Ernietta* from the late Ediacaran Nama Group. Namibia. J. Paleont. 90, 1017–1026.
Evans, S.D., Gehling, J.G., Droser, M.L., 2019. Slime travelers: Early evidence of animal mobility and feeding in an organic mat world. Geobiology 17 (5), 490–509.
Farrell, Ú.C., Martin, M.J., Hagadorn, J.W., Whiteley, T., Briggs, D.E.G., 2009. Beyond Beecher's Trilobite Bed: Widespread pyritization of soft tissues in the Late Ordovician Taconic foreland basin. Geology 37 (10), 907–910.
Fedonkin, M.A., 2002. *Andiva ivantsovi*, gen. et sp. n., and related carapace-bearing Ediacaran fossils from the Vendian of the Winter Coast, White Sea. Russia. Ital. J. Zool. 69 (2), 175–181.
Filippelli, G.M., Carnahan, J.W., Derry, L.A., Kurtz, A., 2000. Terrestrial paleorecords of Ge/Si cycling derived from lake diatoms. Chem. Geol. 168 (1-2), 9–26.
Fisher, I.ST.J., 1986. Pyrite replacement of mollusc shells from the lower Oxford Clay (Jurassic) of England. Sedimentology 33 (4), 575–585.
Furutani, M., Suzuki, T., Ishihara, H., Hashimoto, H., Kunoh, H., Takada, J., 2011. Initial assemblage of bacterial saccharic fibrils and element deposition to form an immature sheath in cultured *Leptothrix* sp. strain OUMS1. Minerals 1 (1), 157–166.
Gabbott, S.E., Xian-guang, H., Norry, M.J., Siveter, D.J., 2004. Preservation of Early Cambrian animals of the Chengjiang biota. Geology 32 (10), 901. https://doi.org/10.1130/G20640.1.
Gaines, R.R., Briggs, D.E.G., Yuanlong, Z., 2008. Cambrian Burgess Shale–type deposits share a common mode of fossilization. Geology 36 (10), 755. https://doi.org/10.1130/G24961A.1.
Gámez Vintaned, J.A., Liñán, E., Zhuravlev, A.Y., 2011. A new early Cambrian lobopod-bearing animal (Murero, Spain) and the problem of the ecdysozoan early diversification. In Pontarotti, P. (ed.), Evolutionary Biology: Concepts, Biodiversity, Macroevolution and Genome Evolution. Berlin, Springer-Verlag, 193–219.
Gan, T., Luo, T., Pang, K., Zhou, C., Zhou, G., Wan, B., Li, G., Yi, Q., Czaja, A.D., Xiao, S., 2021. Cryptic terrestrial fungus-like fossils of the early Ediacaran Period. Nature Comm. 12, 1–12.
Gastaldo, R.A., 1992. Regenerative growth in fossil horsetails following burial by alluvium. Hist. Biol. 6 (3), 203–219.
Gehling, J.G., 1999. Microbial mats in terminal Proterozoic siliciclastics: Ediacaran death masks. Palaios 14 (1), 40. https://doi.org/10.2307/3515360.
Gehling, J.G., Narbonne, G.M., Anderson, M.M., 2000. The first named Ediacaran body fossil; *Aspidella terranovica*. Palaeontology 43 (3), 427–456.
Gilmour, C.C., Elias, D.A., Kucken, A.M., Brown, S.D., Palumbo, A.V., Schadt, C.W., Wall, J.D., 2011. Sulfate-reducing bacterium *Desulfovibrio desulfuricans* ND132 as a model for understanding bacterial mercury methylation. Appl. Environ. Microbiol. 77 (12), 3938–3951.
Girard, J.-P., Razanadranorosoa, D., Freyssinet, P., 1997. Laser oxygen isotope analysis of weathering goethite from the lateritic profile of Yaou, French Guiana: paleoweathering and paleoclimatic implications. Appl. Geochem. 12 (2), 163–174.
Glaessner, M.F., 1979. An echiurid worm from the Late Precambrian. Lethaia 12 (2), 121–124.
Glaessner, M.F., Walter, M.R., 1975. New Precambrian fossils from the Arumbera Sandstone, Northern Territory. Alcheringa 1, 59–69.
Gleisner, M., Herbert, R.B., Frogner Kockum, P.C., 2006. Pyrite oxidation by *Acidithiobacillus ferrooxidans* at various concentrations of dissolved oxygen. Chem. Geol. 225 (1-2), 16–29.
Gould, R.E., 1971. *Lyssoxylon grigsbyi*, a cycad trunk from the Upper Triassic of Arizona and New Mexico. Amer. J. Botany 58 (3), 239–248.
Gould, R.E., Delevoryas, T., 1977. The biology of *Glossopteris*: evidence from petrified seed-bearing and pollen-bearing organs. Alcheringa 1 (4), 387–399.
Grazhdankin, D., 2004. Patterns of distribution in the Ediacaran biotas: facies versus biogeography and evolution. Paleobiology 30 (2), 203–221.
Grazhdankin, D.V., Balthasar, U., Nagovitsin, K.E., Kochnev, B.B., 2008. Carbonate-hosted Avalon-type fossils in arctic Siberia. Geology 36 (10), 803. https://doi.org/10.1130/G24946A.1.
Grey, K., Willman, S., 2009. Taphonomy of Ediacaran acritarchs from Australia: significance for taxonomy and biostratigraphy. Palaios 24 (4), 239–256.
Hagadorn, J.W., Fedo, C.M., Waggoner, B.M., 2000. Early Cambrian Ediacaran-type fossils from California. J. Paleont. 74 (4), 731–740.
Hagadorn, J.W., Dott, R.H., Damrow, D., 2002. Stranded on a Late Cambrian shoreline: Medusae from central Wisconsin. Geology 30 (2), 147. https://doi.org/10.1130/0091-7613(2002)030<0147:SOALCS>2.0.CO;210.1130/2002010.
Hall, J.P., Wolberg, D.L., West, S., 1988. Dinosaur-skin impressions from the Fruitland Formation (Campanian–Maastrichtian) of the Fossil Forest, San Juan Basin, San Juan County, New Mexico. New Mexico Bur. Mines Mineral Res. Bull. 122, 23–27.
Henderson, R.A., 1990. Late Albian ammonites from the Northern Territory, Australia. Alcheringa 14 (2), 109–148.
Hou, X.G., Aldridge, R., Bergstrom, J., Siveter, D.J., Siveter, D., Feng, X.H., 2008. The Cambrian fossils of Chengjiang, China: the flowering of early animal life. Wiley, Chichester, p. 249.
Huldtgren, T., Cunningham, J.A., Yin, C., Stampanoni, M., Marone, F., Donoghue, P.C. J., Bengtson, S., 2011. Fossilized nuclei and germination structures identify Ediacaran "animal embryos" as encysting protists. Science 334 (6063), 1696–1699.
Hurtgen, M.T., Arthur, M.A., Halverson, G.P., 2005. Neoproterozoic sulfur isotopes, the evolution of microbial sulfur species, and the burial efficiency of sulfide as sedimentary pyrite. Geology 33 (1), 41. https://doi.org/10.1130/G20923.110.1130/2005005.
Ichaso, A.A., Dalrymple, R.W., Narbonne, G.M., 2007. Paleoenvironmental and basin analysis of the late Neoproterozoic (Ediacaran) upper Conception and St.John's Groups, west Conception Bay. Newfoundland. Canad. J. Earth Sci. 44 (1), 25–41.
Ivantsov, A.Y., Narbonne, G.M., Trusler, P.W., Greentree, C., Vickers-Rich, P., 2016. Elucidating Ernietta: new insights from exceptional specimens in the Ediacaran of Namibia. Lethaia 49 (4), 540–554.
Jensen, S., Gehling, J.G., Droser, M.L., 1998. Ediacara-type fossils in Cambrian sediments. Nature 393 (6685), 567–569.
Karowe, A.L., Jefferson, T.H., 1987. Burial of trees by eruptions of Mount St Helens, Washington: implications for the interpretation of fossil forests. Geol. Mag. 124 (3), 191–204.
Kaufman, M.H., McNeil, R., 1989. Death masks and life masks at Edinburgh University. Brit. Med. J. 298 (6672), 506–507.
Kurtz, A.C., Derry, L.A., Chadwick, O.A., 2002. Germanium-silicon fractionation in the weathering environment. Geochim. Cosmochim. Acta 66 (9), 1525–1537.
Larkin, J.M., Strohl, W.R., 1983. *Beggiatoa*, *Thiothrix*, and *Thioploca*. Ann. Rev. Microbiol. 37 (1), 341–367.
Leo, R.F., Barghoorn, E.S., 1976. Silicification of wood. Harvard Bot. Mus. Leaflets 25, 1–47.
Linnemann, U., Pidal, A.P., Hofmann, M., Drost, K., Quesada, C., Gerdes, A., Marko, L., Gärtner, A., Zieger, J., Ulrich, J., Krause, R., 2018. A∼ 565 Ma old glaciation in the Ediacaran of peri-Gondwanan West Africa. Int. J. Earth Sci. 107, 885–911.
Liivamägi, S., Somelar, P., Mahaney, W.C., Kirs, J., Vircava, I., Kirsimäe, K., 2014. Late Neoproterozoic Baltic paleosol: Intense weathering at high latitude? Geology 42 (4), 323–326.
Liivamägi, S., Somelar, P., Vircava, I., Mahaney, W.C., Kirs, J., Kirsimäe, K., 2015. Petrology, mineralogy and geochemical climofunctions of the Neoproterozoic Baltic paleosol. Precambrian Res. 256, 170–188.
Liu, A.G., 2016. Framboidal pyrite shroud confirms the 'death mask' model for moldic preservation of Ediacaran soft-bodied organisms. Palaios 31 (5), 259–274.
Liu, A.G., Mcilroy, Duncan, Antcliffe, J.B., Brasier, M.D., 2011. Effaced preservation in the Ediacara biota and its implications for the early macrofossil record. Palaeontology 54 (3), 607–630.
Liu, P., Xiao, S., Yin, C., Chen, S., Zhou, C., Li, M., 2014. Ediacaran acanthomorphic acritarchs and other microfossils from chert nodules of the Upper Doushantuo Formation in the Yangtze Gorges Area, South China. J. Paleont. 88 (S72), 1–139.
Liu, A.G., McMahon, S., Matthews, J.J., Still, J.W., Brasier, A.T., 2019. Petrological evidence supports the death mask model for the preservation of Ediacaran soft-bodied organisms in South Australia. Geology 47 (3), 215–218.
Locatelli, E.R., McMahon, S., Bilger, H., 2017. Biofilms mediate the preservation of leaf adpression fossils by clays. Palaios 32, 708–724.
Luther, G.W., 1987. Pyrite oxidation and reduction: Molecular orbital theory considerations. Geochim. Cosmochim. Acta 51 (12), 3193–3199.
Luther, G.W., Giblin, A., Howarth, R.W., Ryans, R.A., 1982. Pyrite and oxidized iron mineral phases formed from pyrite oxidation in salt marsh and estuarine sediments. Geochim. Cosmochim. Acta 46 (12), 2665–2669.
Lyons, T.W., Reinhard, C.T., Planavsky, N.J., 2014. The rise of oxygen in Earth's early ocean and atmosphere. Nature 506 (7488), 307–315.
MacGabhann, B.A., Schiffbauer, J.D., Hagadorn, J.W., Van Roy, P., Lynch, E.P., Morrison, L., Murray, J., 2019. Resolution of the earliest metazoan record: Differential taphonomy of Ediacaran and Paleozoic fossil molds and casts. Palaeogeogr. Palaeoclim. Palaeoec. 513, 146–165.
Mamay, S.H., 1989. *Evolsonia*, a new genus of Gigantopteridaceae from the Lower Permian Vale Formation, north-central Texas. Amer. J. Botany 76 (9), 1299–1311.
Manchester, S.R., 1994. Fruits and seeds of the middle Eocene Nut Beds flora, Clarno Formation, Oregon. Palaeontographica Americana 58, 1–205.
Manchester, S.R., Dilcher, D.L., Judd, W.S., Corder, B., Basinger, J.F., 2018. Early eudicot flower and fruit: *Dakotanthus* gen. nov. from the Cretaceous Dakota Formation of Kansas and Nebraska, USA. Acta Palaeobotanica 58, 27–40.

Mapstone, N.B., McIlroy, D., 2006. Ediacaran fossil preservation: taphonomy and diagenesis of a discoid biota from the Amadeus Basin, central Australia. Precambrian Res. 149 (3-4), 126–148.
Martill, D.M., 1990. Macromolecular resolution of fossilized muscle tissue from an elopomorph fish. Nature 346 (6280), 171–172.
Martill, D.M., Wilby, P.R., 1994. Lithified prokaryotes associated with fossil soft tissues from the Santana Formation (Cretaceous) of Brazil. Kaupia 2, 71–77.
Marynowski, Leszek, Rakocinski, Michal, Zaton, Michal, 2007. Middle Famennian (Late Devonian) interval with pyritized fauna from the Holy Cross Mountains (Poland): organic geochemistry and pyrite framboid diameter study. Geochem. J. 41 (3), 187–200.
Matten, L.C., 1973. Preparation of pyritized plant petrifactions: "a plea for pyrite". Rev. Palaeobot. Palynol. 16 (3), 165–173.
Matthews, J.J., Liu, A.G., Yang, C., McIlroy, D., Levell, B., Condon, D.J., 2020. A chronostratigraphic framework for the rise of the Ediacaran macrobiota: new constraints from Mistaken Point Ecological Reserve. Newfoundland. Geol. Soc. Amer. Bull. 133, 612–624.
Matysová, P., Rössler, R., Götze, J., Leichmann, J., Forbes, G., Taylor, E.L., Sakala, J., Grygar, T., 2010. Alluvial and volcanic pathways to silicified plant stems (Upper Carboniferous–Triassic) and their taphonomic and palaeo-environmental meaning. Palaeogeogr. Palaeoclim. Palaeoecol. 292 (1-2), 127–143.
Mawson, D., Segnit, E.R., 1949. Purple slates of the Adelaide System. Roy. Soc. South Australia Trans. 72, 276–280.
McMahon, W.J., Liu, A.G., Tindal, B.H., Kleinhans, M.G., 2020. Ediacaran life close to land: Coastal and shoreface habitats of the Ediacaran macrobiota, the Central Flinders Ranges, South Australia. J. Sedim. Res. 90, 1463–1499.
McNamara, K.J., Trewin, N.H., 1993. A euthycarcinoid arthropod from the Silurian of Western Australia. Palaeontology 36, 319–335.
Mortlock, R.A., Froelich, P.N., Feely, R.A., Massoth, G.J., Butterfield, D.A., Lupton, J.E., 1993. Silica and germanium in Pacific Ocean hydrothermal vents and plumes. Earth Planet. Sci. Lett. 119 (3), 365–378.
Moses, C.O., Kirk Nordstrom, D., Herman, J.S., Mills, A.L., 1987. Aqueous pyrite oxidation by dissolved oxygen and by ferric iron. Geochim. Cosmochim. Acta 51 (6), 1561–1571.
Murata, K.J., 1940. Volcanic ash as a source of silica for the silicification of wood. Amer. J. Sci. 238, 586–596.
Murray, R.W., Buchholtz Ten Brink, M.R., Gerlach, D.C., Russ, G.P., Jones, D.L., 1991. Rare earth, major, and trace elements in chert from the Franciscan Complex and Monterey Group, California: Assessing REE sources to fine-grained marine sediments. Geochim. Cosmochim. Acta 55 (7), 1875–1895.
Nishida, H., Pigg, K.B., Kudo, K., Rigby, J.F., 2004. Zooidogamy in the late Permian genus *Glossopteris*. J. Plant Res. 117 (4), 323–328.
Ohfuji, H., Boyle, A.P., Prior, D.J., Rickard, D., 2005. Structure of framboidal pyrite: an electron backscatter diffraction study. American Mineralogist 90, 1693–1704.
Paik, I.S., Kim, H.J., Huh, M., 2010. Impressions of dinosaur skin from the Cretaceous Haman Formation in Korea. J. Asian Earth Sci. 39 (4), 270–274.
Paterson, J.R., García-Bellido, D.C., Lee, M.S.Y., Brock, G.A., Jago, J.B., Edgecombe, G.D., 2011. Acute vision in the giant Cambrian predator Anomalocaris and the origin of compound eyes. Nature 480 (7376), 237–240.
Pellegrin, Véronique, Juretschko, S., Wagner, M., Cottenceau, G., 1999. Morphological and biochemical properties of a *Sphaerotilus* sp. isolated from paper mill slimes. Appl. Environ. Microbiol. 65 (1), 156–162.
Percival, C.J., 1983. The Firestone Sill ganister, Namurian, northern England—the A2 horizon of a podzol or podzolic paleosol. Sediment. Geol. 36, 41–49.
Perkins, W.G., 1998. Timing of formation of Proterozoic stratiform fine-grained pyrite; post-diagenetic cleavage replacement at Mount Isa? Econ. Geol. 93 (8), 1153–1164.
Pflug, H.D., 1973. Zur fauna der Nama-Schichten in Südwest Africa IV. Mikroscopische anatomie der petaloorganism. Palaeontographica B144, 166–202.
Pflug, H.D., 1994. Role of size increase in Precambrian organismic evolution. Neues Jb. Geol. Paläont. Abhandl. 193, 245–286.
Reid, L.M., García-Bellido, D.C., Payne, J.L., Runnegar, B., Gehling, J.G., 2017. Possible evidence of primary succession in a juvenile-dominated Ediacara fossil surface from the Flinders Ranges, South Australia. Palaeogeogr. Palaeoclim. Palaeoec. 476, 68–76.
Retallack, G.J., 1977. Triassic paleosols in the upper Narrabeen Group of New South Wales. Part I: Features of the paleosols. Geol. Soc. Australia J. 23, 383–399.
Retallack, G., 1984. Completeness of the rock and fossil record: some estimates using fossil soils. Paleobiology 10 (1), 59–78.
Retallack, G.J., 1991. Untangling the effects of burial alteration and ancient soil formation. Ann. Rev. Earth Planet. Sci. 19 (1), 183–206.
Retallack, G.J., 1994. Were the Ediacaran fossils lichens? Paleobiology 20 (4), 523–544.
Retallack, G.J., 1997. A color guide to paleosols. Wiley, Chichester, p. 246.
Retallack, G.J., 2007. Decay, growth, and burial compaction of Dickinsonia, an iconic Ediacaran fossil. Alcheringa 31, 215–240.
Retallack, G.J., Kirby, M.X., 2007. Middle Miocene global change and paleogrography of Panama. Palaios 22, 667–679.
Retallack, G.J., 2008. Cambrian paleosols and landscapes of South Australia. Austral. J. Earth Sci. 55 (8), 1083–1106.
Retallack, G.J., 2009. Cambrian-Ordovician non-marine fossils from South Australia. Alcheringa 33 (4), 355–391.
Retallack, G.J., 2010. Lateritization and bauxitization events. Econ. Geol. 105 (3), 655–667.
Retallack, G.J., 2011. Exceptional fossil preservation during CO_2 greenhouse crises? Palaeogeogr. Palaeclim. Paleoecol. 307 (1-4), 59–74.
Retallack, G.J., 2012. Were Ediacaran siliciclastics of South Australia coastal or deep marine? Sedimentology 59 (4), 1208–1236.
Retallack, G.J., 2013a. Early Cambrian humid, tropical paleosols from Montana. In Driese, S.G. (ed.), New Frontiers in Paleopedology and Terrestrial Paleoclimatology. Soc. Econ. Paleont. Mineral. Spec. Pap. 44, 257–272.
Retallack, G.J., 2013b. Ediacaran life on land. Nature 493 (7430), 89–92.
Retallack, G.J., 2014. Volcanosedimentary paleoenvironments of Ediacaran fossils in Newfoundland. Geol. Soc. Amer. Bull. 126 (5-6), 619–638.
Retallack, G.J., 2015. Reassessment of the Silurian problematicum Rutgersella as another post-Ediacaran vendobiont. Alcheringa 39 (4), 573–588.
Retallack, G.J., 2016a. Field and laboratory tests for recognition of Ediacaran paleosols. Gondwana Res. 36, 107–123.
Retallack, G.J., 2016b. Ediacaran fossils in petrographic thin section. Alcheringa 40, 593–600.
Retallack, G.J., 2016c. Ediacaran sedimentology and paleoecology of Newfoundland reconsidered. Sediment. Geol. 333, 15–31.
Retallack, G.J., 2017. Exceptional preservation of soft-bodied Ediacara Biota promoted by silica-rich oceans. Geology 44, e407.
Retallack, G.J., 2018. *Reassessement* of the Devonian Problematicum *Protonympha* as another post Ediacaran vendobiont. Lethaia 51, 406–423.
Retallack, G.J., 2019. Interflag sandstone laminae, a novel fluvial sedimentary structure with implication for Ediacaran paleoenvironments. Sediment. Geol. 379, 60–76.
Retallack, G., 2020. Boron paleosalinity proxy for deeply buried Paleozoic and Ediacaran fossils. Palaeogeogr. Palaeoclim. Palaeoec. 540, 109536. https://doi.org/10.1016/j.palaeo.2019.109536.
Retallack, G.J., 2022. Towards a glacial subdivision of the Ediacaran Period, with an example of the Boston Bay Group, Massachusetts. Austral J. Earth Sci. 69 (2), 223–250.
Retallack, G.J., Broz, A., 2020a. *Arumberia* and other Ediacaran fossils from central Australia. Hist. Biol. 32, 1755281.
Retallack, G.J., Broz, A., 2020b. Ediacaran and Cambrian paleosols in central Australia. Palaeogeogr. Palaeoclim. Palaeoec. 560, 110047.
Retallack, G.J., Dilcher, D.L., 2012. Outcrop versus core and geophysical log interpretation of mid-Cretaceous paleosols from the Dakota Formation of Kansas. Palaeogeogr. Palaeoclim. Palaeoec. 329-330, 47–63.
Retallack, G.J., Marconato, A., Osterhout, J.T., Watts, K.E., Bindeman, I.N., 2014. Revised Wonoka isotopic anomaly in South Australia and Late Ediacaran mass extinction. J. Geol. Soc. London 171 (5), 709–722.
Retallack, G.J., Matthews, N.A., Master, S., Khangar, R.G., Khan, M., 2021. *Dickinsonia* discovered in India and late Ediacaran biogeography. Gondwana Res. 90, 165–170.
Rice, C.M., Trewin, N.H., Anderson, L.I., 2002. Geological setting of the Early Devonian Rhynie cherts, Aberdeenshire, Scotland: an early terrestrial hot spring system. Geol. Soc. London J. 159 (2), 203–214.
Richmond, K.E., Sussman, M., 2003. Got silicon? The nonessential beneficial plant nutrient. Current Opinion Plant Biology 6 (3), 268–272. https://doi.org/10.1016/S1369-5266(03)00041-4.
Rimstidt, J.D., Vaughan, D.J., 2003. Pyrite oxidation: A state-of-the-art assessment of the reaction mechanism. Geochim. Cosmochim. Acta 67 (5), 873–880.
Rothwell, G.W., 1972. Evidence of pollen tubes in Paleozoic pteridosperms. Science 175 (4023), 772–774.
Schiffbauer, J.D., Selly, T., Jacquet, S.M., Merz, R.A., Nelson, L.L., Strange, M.A., Cai, Y., Smith, E.F., 2020. Discovery of bilaterian-type through-guts in cloudinomorphs from the terminal Ediacaran Period. Nature Comm. 11, 1–12.
Schopf, J.M., 1975. Modes of fossil preservation. Rev. Palaeobot. Palynol. 20 (1-2), 27–53.
Seilacher, A., 1989. Vendozoa: organismal construction in the Proterozoic biosphere. Lethaia 22, 229–239.
Seilacher, A., 1999. Biomat-related lifestyles in the Precambrian. Palaios 14 (1), 86. https://doi.org/10.2307/3515363.
Shen, B., Lee, C.-T., Xiao, S., 2011. Germanium/silica ratios in diagenetic chert nodules from the Ediacaran Doushantuo Formation, South China. Chem. Geol. 280 (3-4), 323–335.
Sigleo, A.C., 1978. Degraded lignin compounds in silicified wood 200 million years old. Science 200, 1054–1056.
Sigleo, A.C., 1979. Geochemistry of silicified wood and associated sediments, Petrified Forest National Park. Arizona. Chem. Geol. 26 (1-2), 151–163.
Silverman, M.P., 1967. Mechanism of bacterial pyrite oxidation. J. Bacteriol. 94 (4), 1046–1051.
Smith, E.F., Nelson, L.L., Strange, M.A., Eyster, A.E., Rowland, S.M., Schrag, D.P., Macdonald, F.A., 2016. The end of the Ediacaran: Two new exceptionally preserved body fossil assemblages from Mount Dunfee, Nevada, USA. Geology 44 (11), 911–914.
Spicer, R.A., 1977. The pre-depositional formation of some leaf impressions. Palaeontology 20, 907–912.
Slagter, S., Tarhan, L.G., Hao, W., Planavsky, N.J., Konhauser, K.O., 2020. Experimental evidence supports early silica cementation of the Ediacara Biota. Geology 49, 51–55.
Steiner, M., Reitner, J., 2001. Evidence of organic structures in Ediacara-type fossils and associated microbial mats. Geology 29 (12), 1119. https://doi.org/10.1130/0091-7613(2001)029<1119:EOOSIE>2.0.CO;2.

Street-Perrott, F.A., Barker, P.A., 2008. Biogenic silica: a neglected component of the coupled global continental biogeochemical cycles of carbon and silicon. Earth Surface Processes Landforms 33 (9), 1436–1457.
Struve, W., 1985. Versetzung der Art Phacops schmidti in die Gattung Denckmannites. Senckenbergiana Lethaia 65, 433–441.
Tarhan, L.G., Droser, M.L., Gehling, J.G., 2015. Depositional and preservational environments of the Ediacara Member, Rawnsley Quartzite (South Australia): Assessment of paleoenvironmental proxies and the timing of 'ferruginization'. Precambrian Res. 434, 4–13.
Tarhan, L.G., Hood, A.v.S., Droser, M.L., Gehling, J.G., Briggs, D.E.G., 2016. Exceptional preservation of soft-bodied Ediacara biota promoted by silica-rich oceans. Geology 44 (11), 951–954.
Tarhan, L.G., Droser, M.L., Gehling, J.G., Dzaugis, M.P., 2017. Microbial mat sandwiches and other anactualistic sedimentary features of the Ediacara Member (Rawnsley Quartzite, South Australia): implications for interpretation of the Ediacaran sedimentary record. Palaios 32 (3), 181–194.
Tarhan, L.G., Planavsky, N.J., Wang, X., Bellefroid, E.J., Droser, M.L., Gehling, J.G., 2018. The late-stage "ferruginization" of the Ediacara Member (Rawnsley Quartzite, South Australia): Insights from uranium isotopes. Geobiology 16 (1), 35–48.
Tarhan, L.G., Hood, A.V.S., Droser, M.L., Gehling, J.G., Briggs, D.E.G., Gaines, R.R., Robbins, L.J., Planavsky, N.J., 2019. Petrological evidence supports the death mask model for the preservation of Ediacaran soft-bodied organisms in South Australia: Comment. Geology 47 (8), e473.
Thauer, R.K., Stackebrandt, E., Hamilton, W.A., 2007. Energy metabolism and phylogenetic diversity of sulphate-reducing bacteria. In: Barton, L.L., Hamilton, W.A. (Eds.), Sulphate-Reducing Bacteria: Environmental and Engineered Systems. Cambridge University Press, pp. 1–38. https://doi.org/10.1017/CBO9780511541490.002.
Thomas, B.P., Fitzpatrick, R.W., Merry, R.H., Poch, R.M., Hicks, W.S., Raven, M.D., 2004. Contemporary and relict processes in a coastal acid sulfate soil sequence: macroscopic and geomorphic features. SuperSoil 2004 Australian New Zealand Soil Conf. 3, 1–8.
Tidwell, W.D., Simper, A.D., Thayn, G.F., 1977. Additional information concerning the controversial Triassic plant; *Sanmiguelia*. Palaeontographica B163, 143–151.
Trewin, N.H., Knoll, A.H., 1999. Preservation of Devonian chemotrophic filamentous bacteria in calcite veins. Palaios 14 (3), 288. https://doi.org/10.2307/3515441.
van Veen, W.L., Mulder, E.G., Deinema, M.H., 1978. The *Sphaerotilus-Leptothrix* group of bacteria. Microbiol. Rev. 42 (2), 329–356.
Vickers-Rich, P., Ivantsov, A.Y., Trusler, P.W., Narbonne, G.M., Hall, M., Wilson, S.A., Greentree, C., Fedonkin, M.A., Elliott, D.A., Hoffmann, K.H., Schneider, G.I.C., 2013. Reconstructing Rangea: new discoveries from the *Ediacaran* of southern Namibia. J. Paleont. 87, 1–15.
Vickers-Rich, P., Narbonne, G.M., Laflamme, M., Darroch, S., Kaufman, A.J., Kriesfeld, L., 2016. The Nama Group of southern Namibia: the end game of the first large complex organisms on Earth. Field Guide Int. Geol. Congr. Cape Town 87, 1–15.
Voordouw, G., 1995. The Genus *Desulfovibrio*. Centenn. Appl. Environ. Microbiol. 61, 2813–2819.
Wade, Mary, 1968. Preservation of soft-bodied animals in Precambrian sandstones at Ediacara, South Australia. Lethaia 1 (3), 238–267.
Wade, M., 1969. Medusae from uppermost Precambrian or Cambrian sandstones, central Australia. Palaeontology 12, 315–365.
Wan, B., Chen, Z., Yuan, X., Pang, K.e., Tang, Q., Guan, C., Wang, X., Pandey, S.K., Droser, M.L., Xiao, S., 2020. A tale of three taphonomic modes: The Ediacaran fossil *Flabellophyton* preserved in limestone, black shale, and sandstone. Gondwana Res. 84, 296–314.
Wen, H., Fan, H., Tian, S., Wang, Q., Hu, R., 2016. The formation conditions of the early Ediacaran cherts, South China. Chem. Geol. 430, 45–69.
Whalley, P., Jarzembowski, E.A., 1981. A new assessment of *Rhyniella*, the earliest known insect, from the Devonian of Rhynie. Scotland. Nature 291 (5813), 317.
White, M.E., 1991. Time in our Hands. Reed, Balgowlah, p. 191.
Wood, D.A., Dalrymple, R.W., Narbonne, G.M., Gehling, J.G., Clapham, M.E., 2003. Paleoenvironmental analysis of the late Neoproterozoic Mistaken Point and Trepassey formations, southeastern Newfoundland. Canad. J. Earth Sci. 40 (10), 1375–1391.
Wright, W.W., 2002. The Triassic Chinle Formation, U.S.A., and its woods. In: Dernbach, U., Tidwell, W.D. (Eds.), Secrets of Petrified Plants: Fascination from Millions of Years. D'Oro Publishers, Chemnitz, pp. 121–133.
Xiao, Shuhai, 2004. New multicellular algal fossils and acritarchs in Doushantuo chert nodules (Neoproterozoic; Yangtze Gorges, South China). J. Paleont. 78 (2), 393–401.
Xiao, S., Yuan, X., Steiner, M., Knoll, A.H., 2002. Macroscopic carbonaceous compressions in a terminal Proterozoic shale: a systematic reassessment of the Miaohe biota, South China. J. Paleont. 76 (2), 347–376.
Xiao, S., Schiffbauer, J.D., McFadden, K.A., Hunter, J., 2010. Petrographic and SIMS pyrite sulfur isotope analyses of Ediacaran chert nodules: Implications for microbial processes in pyrite rim formation, silicification, and exceptional fossil preservation. Earth Planet. Sci. Lett. 297 (3-4), 481–495.
Xiao, S., Zhou, C., Liu, P., Wang, D., Yuan, X., 2014. Phosphatized acanthomorphic acritarchs and related microfossils from the Ediacaran Doushantuo Formation at Weng'an (South China) and their implications for biostratigraphic correlation. J. Paleont. 88 (1), 1–67.
Yuan, X., Xiao, S., Taylor, T.N., 2005. Lichen-like symbiosis 600 million years ago. Science 308 (5724), 1017–1020.